Remote Sensing of Environment 184 (2016) 212–228

Contents lists available at ScienceDirect

Remote Sensing of Environment

journal homepage: www.elsevier.com/locate/rse

A morphology independent methodology for quantifying planview river change and characteristics from remotely sensed imagery

Joel C. Rowland [a,*], Eitan Shelef [a], Paul A. Pope [b], Jordan Muss [a], Chandana Gangodagamage [a], Steven P. Brumby [c], Cathy J. Wilson [a]

[a] Earth & Environmental Sciences Division, MS-J495, Los Alamos National Laboratory, Los Alamos, NM 87505, United States
[b] Intelligence & Space Research Division, MS-B244, Los Alamos National Laboratory, Los Alamos, NM 87505, United States
[c] Computer, Computational, and Statistical Sciences Division, MS-B244, Los Alamos National Laboratory, Los Alamos, NM 87505, United States

ARTICLE INFO

Article history:
Received 1 October 2015
Received in revised form 3 June 2016
Accepted 6 July 2016
Available online 15 July 2016

Keywords:
Rivers
Change detection
Morphology
Erosion
Accretion

ABSTRACT

Remotely sensed imagery of rivers has long served as a means for characterizing channel properties and detection of planview change. In the last decade the dramatic increase in the availability of satellite imagery and processing tools has created the potential to greatly expand the spatial and temporal scale of our understanding of river morphology and dynamics. To date, the majority of GIS and automated analyses of planview changes in rivers from remotely sensed data has been developed for single-threaded meandering river systems. These methods have limited applicability to many of the earth's rivers with complex multi-channel planforms. Here we present the methodologies of a set of analysis algorithms collectively called Spatially Continuous Riverbank Erosion and Accretion Measurements (SCREAM). SCREAM analyzes planview river metrics regardless of river morphology. These algorithms quantify both the erosion and accretion rates of riverbanks from binary masks of channels generated from imagery acquired at two time periods. Additionally, the program quantifies the area of change between river channels and the surrounding floodplain and area of islands lost or formed between these two time periods. To examine variations in erosion rates in relation to local channel attributes and make rate comparisons between river systems of varying sizes, the program determines channel widths and bank curvature at every bank pixel. SCREAM was developed and tested on rivers with diverse and complex planform morphologies in imagery acquired from a range of observational platforms with varying spatial resolutions. Validation and verification of SCREAM-generated metrics against manual measurements show no significant measurement errors in determination of channel width, erosion, and bank aspects. SCREAM has the potential to provide data for both the quantitative examination of the controls on erosion rates and for the comparison of these rates across river systems ranging broadly in size and planform morphology.

1. Introduction

The analysis of river planform properties and dynamics has long used aerial photography and increasingly incorporates satellite imagery. Traditionally, extracting a representation of a river, such as banklines or a centerline, relied on labor-intensive efforts by a human analyst to digitize the river channel. The development of supervised and semi-automated methodologies for extracting a binary representation of rivers from pixel-based images (e.g. Brumby et al., 1999; Dey & Bhattacharya, 2013; Dillabaugh, Niemann, & Richardson, 2002; Hamilton, Kellndorfer, Lehner, & Tobler, 2007; Marra, Kleinhans, & Addink, 2014; McFeeters, 1996; Merwade, 2007; Quackenbush, 2004; Smith & Pavelsky, 2008; Xu, 2006) and the wealth of freely available imagery offers the potential to greatly expand both the temporal and spatial scale of river analysis (Fisher, Bookhagen, & Amos, 2013). In response to the greater availability of imagery, expanded use of Geographic Information Systems (GIS) and image processing software packages, a number of published and freely distributed methodologies for extracting river metrics from imagery have become available over the past decade. Examples of such tools include, but are not limited to, the ArcGIS-based River Planform Statistics Toolbox (Aalto, Lauer, & Dietrich, 2008), the Interactive Data Language (IDL)-based RivWidth code (Pavelsky & Smith, 2008), the Matlab-based width and centerline ChanGeom code (Fisher et al., 2013), and Matlab-based channel centerline and curvature codes (Legleiter & Kyriakidis, 2006). Table 1 provides a representative summary of the range of measurements these and other published methodologies generate. The ever-expanding availability of high-resolution topographic data has led to the development of geomorphic change detection (GCD) and DEMs of difference (DoD) methods to quantify both lateral and vertical changes in river systems

* Corresponding author.
E-mail addresses: jrowland@lanl.gov (J.C. Rowland), shelefeitan@gmail.com (E. Shelef), papope@lanl.gov (P.A. Pope), muss@lanl.gov (J. Muss), chhandana@gmail.com (C. Gangodagamage), steven@descarteslabs.com (S.P. Brumby), cjw@lanl.gov (C.J. Wilson).

http://dx.doi.org/10.1016/j.rse.2016.07.005
0034-4257/

Table 1
Summary of representative river analysis methods and metrics.

	Method									
	Planform Statistics Toolbox[a]	RivWidth[b]	ChanGeom[c]	Centerline polygons[d]	Centerline curvature[e]	Area based change[f]	CWT[g]	Outer bank displacement[h]	SCREAM	SCREAM output
Morphology	S	S/M	S	S	S	S/M	M	M	S/M	
Metric										
Linear rates of lateral channel migration	Intervals	–	–	Polygons	–	–	–	–	–	–
Linear rate of bank erosion	–	–	–	–	–	–	–	XS	–	–
									Bank pixel/segment averages	Raster/text
Linear rate of bank accretion	–	–	–	–	–	–	–	–	Bank pixel/segment averages	Raster/text
Area of erosion	–	–	–	–	–	Entire river reach	–	–	Entire river reach/segments	Text
Area of accretion	–	–	–	–	–	Entire river reach	–	–	Entire river reach/segments	Text
Change as % of channel area	–	–	–	–	–	Entire river reach	–	–	Entire river reach/segments	Text
Percentage of banks eroding and accreting	–	–	–	–	–	–	–	–	Segments	Text
Spatial and temporal patterns of bank change	–	–	–	–	–	–	XS	–	–	–
Channel width	Intervals	CP	CP	–	–	–	–	–	Bank pixel/segment averages	Raster/Text
Total width of multi-thread channels	–	CP	–	–	–	–	–	XS	Segment averages	Text
Centerline curvature	Intervals	–	–	–	Continuous	–	–	–	–	–
Bank curvature	–	–	–	–	–	–	–	–	Bank pixel	Raster/text
Bank aspect	–	–	–	–	–	–	–	–	Bank pixel	Raster/text
Sinuosity	–	–	–	–	–	–	–	–	Continuous/segment averages	Text
Channel elongation	Intervals	–	–	–	–	–	–	–	–	–
Number of islands	–	–	–	–	–	–	–	–	Segments	Text
Total island area	–	–	–	–	–	–	–	–	Segments	Text
Total length of banks	–	–	–	–	–	–	–	–	Segments	Text
Total length of island perimeters	–	–	–	–	–	–	–	–	Segments	Text
Number and location of cutoffs and avulsions	–	–	–	–	–	–	–	–	Entire river reach	Text

S — single-thread channel.
M — multi-thread channel.
XS — cross section.
CP — centerline pixel.
[a] Aalto et al. (2008); Lauer & Parker (2008b).
[b] Pavelsky & Smith (2008).
[c] Fisher et al. (2013).
[d] Micheli et al. (2004); Micheli & Kirchner (2002).
[e] Güneralp & Rhoads (2008); Legleiter & Kyriakidis (2006).
[f] Peixoto et al. (2009).
[g] Continuous wavelet transforms; Mount, Tate, Sarker, & Thorne (2012).
[h] Baki & Gan (2012); Hossain, Gan, & Baki (2013).

(James, Hodgson, Ghoshal, & Latiolais, 2012; Wheaton, Brasington, Darby, & Sear, 2010). The temporal and spatial availability of data sets needed for this type of analysis, however, are still limited enough that the analysis of remotely sensed imagery remains a critical tool for studies of multi-temporal river dynamics.

Current methodologies have the potential to add great efficiency to the analysis task of river planview metrics, but a lack of method standardization in river change studies still persists (Hooke, 1980; Lawler, 1993; Peixoto, Nelson, & Wittmann, 2009). This problem arises from variation in data sources, analysis tools, and the objectives of the individual studies. This lack of methodological consistency between studies greatly confounds inter-study comparisons and data compilation efforts. Furthermore, the diversity of metrics used to quantify change complicates the comparison of results of planview river changes between studies. Reported measures include: lateral migration, erosion, accretion, area change as a percentage of river area, change in area per unit river length, river path length, sinuosity, curvature, radius of curvature, width, and areal changes in river channel position (Table 1). Bank erosion and channel migration rates represent the most commonly reported metrics and can be, but are not necessarily, synonymous. Bank erosion measurements quantify the material removed from the exposed face of a riverbank, and are reported as a linear distance per interval of time (e.g., meter (m) per year (yr)). Channel migration measures the net movement of a channel resulting from the change in river location due to the combined effects of erosion and deposition (Leopold, 1973; Leys & Werritty, 1999).

Numerous studies using remotely sensed data have determined lateral migration rates based on the lateral change in the river centerline position, commonly calculated as the midpoint between opposite banks (e.g. Aalto et al., 2008; Constantine, Dunne, Ahmed, Legleiter, & Lazarus, 2014; Konrad et al., 2011; Lauer & Parker, 2008b; Legleiter & Kyriakidis, 2006; Mount & Louis, 2005; Shields, Simon, & Steffen, 2000) or directly digitized by the analyst (e.g. Brice, 1977; Constantine, Dunne, & Hanson, 2009; Hooke & Harvey, 1983; Hooke & Yorke, 2010; Micheli, Kirchner, & Larsen, 2004; Micheli & Larsen, 2011; Micheli & Kirchner, 2002). For a single-threaded channel with a constant width and no positional errors in

bank location, the change in the position of the centerline should accurately reflect bank erosion (Fig. 1a). Hooke and Yorke (2010) and Parker et al. (2011), however, point out that in many migrating river channels, the erosion and accretion of banks become temporally out of phase. A channel may widen in response to bank erosion followed by a corresponding bank accretion on the opposing bank causing the channel to then narrow resulting in temporal width variations. A centerline derived from a channel in which the position of only one side of the channel has moved over the time interval examined will reflect only half the actual change in the bank erosion (or accretion) (Fig. 1b). Additionally, in river channels experiencing widening or narrowing due to erosion or accretion on both sets of banks, channel migration estimates derived from centerlines will only measure the difference, not the total magnitude, in the widening and narrowing occurring on opposite banks. In a situation where the widening or narrowing occurs equally on opposing banks, there will be no recorded migration of the channel centerline (Fig. 1c). Therefore, in studies and modeling efforts examining the rate of movement of a channel as a whole, migration rates derived from centerlines represent an appropriate and accurate metric. However, in studies that quantify sediment exchange to and from floodplains or the dynamics of bank erosion, migration rates of channel centerlines may not fully capture the dynamics of the system. Additionally, recent advances in modeling of river channel erosion and migration treat the dynamics of opposing banks independently (Asahi, Shimizu, Nelson, & Parker, 2013; Eke, Parker, & Shimizu, 2014; Eke et al., 2014; Parker et al., 2011; Zolezzi, Luchi, & Tubino, 2012a), thereby necessitating measurement techniques that quantify bank changes independent of the net movement of the channel centerline.

While effective methodologies have been developed and applied to quantify channel widths in multi-threaded channel systems (Allen & Pavelsky, 2015; Pavelsky & Smith, 2008; Yamazaki et al., 2014), the majority of methods developed for analyzing changes in planview river properties from remotely sensed imagery were developed for and applied to single-threaded meandering channel systems (Table 1). These methods have limited applicability to multi-threaded systems with complex planform geometries. This limitation greatly restricts the size and global extent of river analysis efforts. The earth's mega rivers (as defined by Latrubesse (2008) as having mean annual discharges >17,000 m^3/s), with the exception of the Mississippi River, have complex multi-thread channel patterns (Ashworth & Lewin, 2012; Latrubesse, 2008). Many smaller river systems also have complex multi-threaded channel forms. The limited number of studies that have explored planview change in multi-threaded river systems used varied methods and metrics creating a challenge for inter-river comparisons. For example, Mount et al. (2012) provided a wavelet-based analysis of bank line retreat on the Jamuna River, Bangladesh. This study quantified the displacement of the system's outermost banks normal to the dominant orientation of the river channel belt, but did not examine bank erosion within the network of river channel threads. Similarly, measurements of outer bank displacements of the Jamuna River and the Ganges were made on evenly spaced cross-sections oriented orthogonally to the valley axis (Baki & Gan, 2012; Hossain et al., 2013). Other research on the Jamuna used a network centrality approach to characterize the structure and variability of the channel belt, but did not explore bank erosion rates (Marra et al., 2014). Studies of the Lena River, Russia have measured bank erosion rates and bank movement rates, but the details of the methodology were not described (Costard & Gautier, 2008; Costard et al., 2007; Gautier, Brunstein, Costard, & Lodina, 2003).

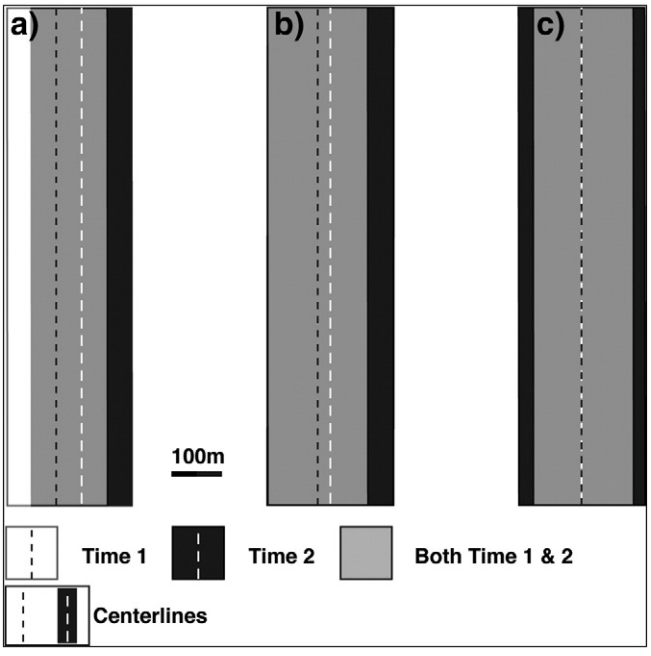

Fig. 1. Three hypothetical changes in channel position between Time 1 and Time 2 having equal areas of erosion of the bounding floodplain but differing channel centerline migration (dashed lines). a) The channel shifts laterally 50 m, with equal areas of erosion and deposition on opposite sides of the channel. b) The channel at Time 2 widens by 50 m on one side; the average linear erosion along the banks is 50 m, but the migration of channel centerlines is only 25 m. c) The channel widens by 50 m by eroding 25 m along each channel margin. The total erosion along the channel is the same as a and b, but the migration of the centerline indicates 0 m of change.

Motivated by the need to measure planview changes of complex multi-threaded rivers, we developed a set of algorithms to analyze these changes using aerial photographs and satellite imagery. We have named this set of algorithms Spatially Continuous Riverbank Erosion & Accretion Measurements (SCREAM). Given the importance of bank properties (Thorne & Tovey, 1981) and the local flow conditions (Darby et al., 2010; Kean & Smith, 2006a, 2006b) on bank erosion rates, and the challenge of delineating centerlines in multi-threaded rivers, we adopted a bank-centered reference frame for measuring change. SCREAM generates a suite of measurements related to planview attributes of the channel, such as width, bank curvature, sinuosity, and bank aspects, as well as, metrics to quantify changes in channel and floodplain area and linear rates of changes in bank position over time (Table 1). These metrics may be determined at a scale as fine as the pixel resolution of the input imagery, and binned in regularly spaced intervals along the channel for examination of spatial patterns of river morphology and dynamics. Table 1 summarizes additional metrics related to planview characteristics of rivers calculated by SCREAM.

This paper aims to provide a clear description of the methodologies used to generate the range of metrics output by the SCREAM algorithms. This description will aid in the proper use of SCREAM by other researchers and allow for critical evaluation of the unique set SCREAM-generated outputs in future studies of river morphology and dynamics. Following the description of SCREAM methodologies, we apply SCREAM to a range of natural river systems to illustrate the output and place the metrics in the context of previously published methods and remote sensing based studies of rivers. We present an accuracy assessment of these example results by comparing SCREAM results to manually derived measurements. We supplement the results of this accuracy assessment with a comparison of SCREAM against existing algorithms for the measurement of lateral river channel migration, river channel curvature, and channel width. These comparisons allow for the evaluation of the comparability of SCREAM metrics relative to alternative methodologies and provide additional confidence in the reliability of SCREAM output. We conclude with a discussion of what we perceive to be the relative strengths and limitations of SCREAM and areas for future evaluation and code refinement.

2. Methods

SCREAM incorporates a collection of scripts written in IDL, a commercially available software package licensed by ExelisVis. IDL-based

applications may be run using the IDL Virtual Machine without a license. SCREAM requires two georeferenced binary masks of the river channel at two successive dates with pixels projected onto a common uniform grid of identical dimensions and resolutions. In these masks, river channel pixels have a value of one while all non-river channel pixels equal zero. Rather than digitizing the extents of river channels from imagery, we derived the channel masks from automated feature extraction software trained to identify river pixels in remotely sensed imagery. Mask generation occurs outside of SCREAM and the choice of masking methodology is not critical to the use of SCREAM. Binary masks of river channels may be generated using a variety of techniques (Brumby et al., 1999; Dey & Bhattacharya, 2013; Dillabaugh et al., 2002; Fisher et al., 2013; Hamilton et al., 2007; Marra et al., 2014; McFeeters, 1996; Merwade, 2007; Quackenbush, 2004; Smith & Pavelsky, 2008; Xu, 2006; Zolezzi, Luchi, & Tubino, 2012b) though ones that rely on a spectral threshold for water to define the channel may suffer errors in estimating consistent bankfull extents with imagery acquired at times of differing river stages. However, if a user inputs river masks derived from the wetted extent of a river at different times with varying river stages, from other data sources, SCREAM could be used to calculate stage–area relationships useful for estimation of river discharge or hydrological modeling (Gleason & Smith, 2014; Smith & Pavelsky, 2008).

To minimize errors in bankfull channel extent associated with variations in river stage we extracted river channels based on criteria aimed at identifying the physical boundaries of the channel (Fig. 2a). In our classification, we considered both open water and bare sand/gravel as river channel, while vegetated pixels were classified as non-river. Numerous prior studies of river channels have used this classification approach to delineate bankfull channel extents independent of river stage (Aalto et al., 2008; Fisher et al., 2013; Gurnell, 1997a; Gurnell, 1997b; Lauer & Parker, 2008b; Mount & Louis, 2005; Peixoto et al., 2009; Richard, Julien, & Baird, 2005; Winterbottom & Gilvear, 2000). While seasonal changes in vegetation cover and overhanging vegetation potentially result in uncertainty in the delineation of channel banks (Gurnell, 1997b; Mount & Louis, 2005), this method generally provides a consistent set of criteria for defining channel extents independent of river discharge. This approach inherently assumes that any region or bank within the channel that has exposed sediment experiences flow and sediment transport frequently enough to inhibit the colonization of vegetation. Therefore it experiences flow at time intervals that are within the common hydrological definition of bankfull flow (at least once every few years) (Knighton, 1998). In arid regions or other areas with sparse vegetation or infrequent channel clearing flows this assumption requires careful consideration.

To derive the binary channel masks used in this study, we used the supervised automated feature extraction software package GeniePro (Brumby et al., 1999; Perkins et al., 2005) which is commercially available from Observera Inc. and allows for the automated delineation of the full extent of a river channel (wetted and dry exposed portions of the channel bed) using all available spectral bands of the imagery based on a user defined set of training data. In addition to spectral content, GeniePro uses spatial context of pixels in the user-defined training regions to identify distinct features within the imagery and can be trained to identify boundaries with variable attributes such as shadowing and vegetation. In our experience, GeniePro largely, but not completely, avoids the four significant hurdles to automated feature extraction of river channels raised by Priestnall and Aplin (2006): 1) determining the edge of the river; 2) channel boundaries obscured by vegetation or shadows; 3) confusion with other linear features; and 4) context.

Automated channel delineations were followed by manual edits to remove classification errors, eliminate areas affected by overhanging trees (evidenced by local outward irregularities in the bank lines and visibly tilted trees) and to trim fragments of tributary channels connected to the master channel of interest.

In addition to providing input rasters, the user needs to specify the dates of the imagery (in decimal years) and identify the corner of the raster closest to the upstream end of the channel mask. If the upstream end of the channel is near the middle of a raster boundary, then either corner of that boundary may be specified. Program options include: the ability to segment the channel rasters to calculate river change and attributes at regularly spaced intervals; specification of the interval length; and the selection of a common reference frame for multi-temporal analyses by providing an existing raster-based channel centerline for use in channel segmentation.

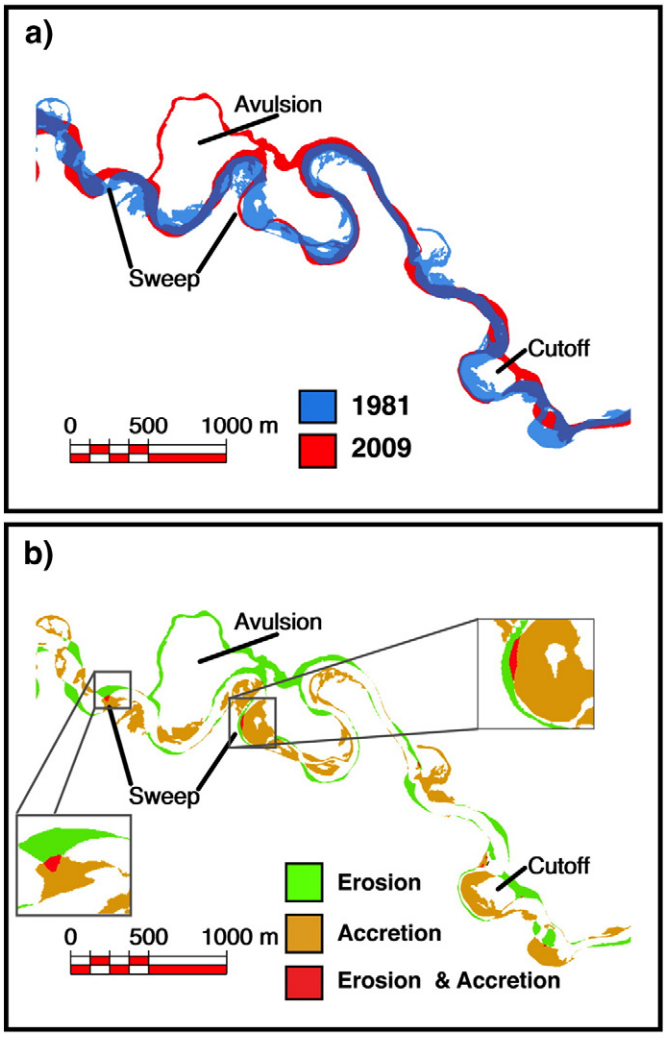

Fig. 2. a) Two binary masks of a portion of the Selawik River, Alaska derived from September 24 and 29, 2009 Geoeye images (red) and July 25, 1981 Alaska High Altitude Photography (AHAP) (blue). Areas of red not overlain by the blue mask represent areas of the floodplain that eroded. Areas labeled "Sweep" mark places where the channel eroded more than a channel width. Areas where the channel jumped to a new location are labeled as "Avulsion" or "Cutoff". b) Areas experiencing erosion, accretion, and both erosion and accretion.

2.1. Delineating areas of change between time periods

SCREAM generates a map of change in a river channel location between the acquisition dates of the two images by differencing the two input rasters (Fig. 2). Subtracting the Time 1 channel mask from the Time 2 channel mask generates a resultant raster with values of −1 for regions of channel accretion, 0 for no change, and 1 for erosion. Based on these values, SCREAM creates two separate change masks: erosion and accretion. Similar approaches were employed in studies of river planview change in the Amazon basin using a raster-based approach (Peixoto et al., 2009; Rozo, Nogueira, & Castro, 2014), and

Gurnell, Downward, and Jones (1994) used a comparable polygon-based approach. Each mask is analyzed separately but in an identical manner to quantify erosion and accretion, respectively. SCREAM uses the number of pixels in each of the erosion/accretion regions to quantify areas of change and these measurements can be binned at regular intervals along the river channel (Section 2.5).

In a number of unique cases, the SCREAM analysis requires additional constraints to accurately measure erosion and accretion. If a river channel migrates more than a full channel width over the time interval between image acquisition, there will be regions of the mask that show no change between the two images but have in fact changed from non-river to river and back to non-river over this time period (Fig. 2). This issue has also confounded prior area-based analyses of planview change in rapidly migrating rivers (Peixoto et al., 2009; Shields et al., 2000).

Identification of the regions where the channel has migrated more than a channel width becomes further complicated by instances in which the channel moves significant distances across the floodplain by abrupt jumps (cutoffs and avulsions) rather than continuous migration. The identification of such regions requires several screening steps. Areas undergoing both erosion and accretion can be identified because the river channel pixels fully enclose them when the river masks from the two time intervals are combined (Fig. 2 — areas labeled "sweep"), but islands present at both time periods also meet this criteria. SCREAM, however, labels the islands in the initial input masks and excludes those pixels from further consideration. Next, to differentiate between areas over which the river continuously swept from Time 1 to Time 2 from areas where the river abruptly changed location through cutoff or avulsion, SCREAM compares the average distance across the possible area of change to the average local width of the channels bounding this area. SCREAM calculates this average distance by dividing the area of the region by half of the area's perimeter length (Micheli et al., 2004). If the average distance across this bounded region is less than a user specified threshold (in units of local channel widths), that is based on the size of the river, the rates of migration expected, and the time interval examined, then the change is considered to be a region where the channel has swept across the floodplain and SCREAM adds this area to both the erosion and accretion masks (red regions in Fig. 2b). If the distance is greater than the threshold SCREAM marks these areas as either a cutoff or avulsion.

Prior to differencing the channel masks, SCREAM performs a filtering operation to remove the smallest islands in the mask. Changes associated with these features are the least accurate because they have the greatest relative error in terms of the number of potentially misclassified pixels (Supplementary data). The default filter threshold removes islands with areas smaller than the island area corresponding to the 0.01 percentile in the cumulative distribution of island sizes. The threshold was selected by trial and error to get rid of very small islands (a few pixels in size). To prevent the removal of significant islands in a river with a very uniform distribution of island sizes, a river must have >10 islands and the standard deviation in island sizes must be more than half the mean island size for filtering to be performed.

After differencing the masks, SCREAM also filters out single isolated pixels prior to calculating change in bank locations and channel areas, similar to the approach of Serra, Pons, and Sauri (2003). As with small islands, changes associated with a single pixel have the potential to have errors of similar magnitudes to the measured change due to both misregistration of imagery and/or classification errors (Supplementary data).

2.2. Linear rates of change

To examine the patterns and rates of change at the pixel scale and to generate metrics comparable to prior studies, we calculate linear rates of bank erosion and accretion in units of (length (L) / time (T)) for every bank pixel in the input raster. The length used in these rates is the distance from a bank pixel at Time 1 to the closest bank pixel at Time 2 that borders the same region of channel change (Section 2.1) (Fig. 3a). SCREAM employs identical methods for calculating rates of erosion and accretion, using separate erosion and accretion change masks.

SCREAM identifies the riverbank pixels by subtracting the input river masks from a copy of the river mask dilated (expanded) by one pixel. This operation will create two bank segments (a series of laterally adjacent pixels) on either side of a single-thread river with no islands, but may delineate numerous unique bank segments for complex braided

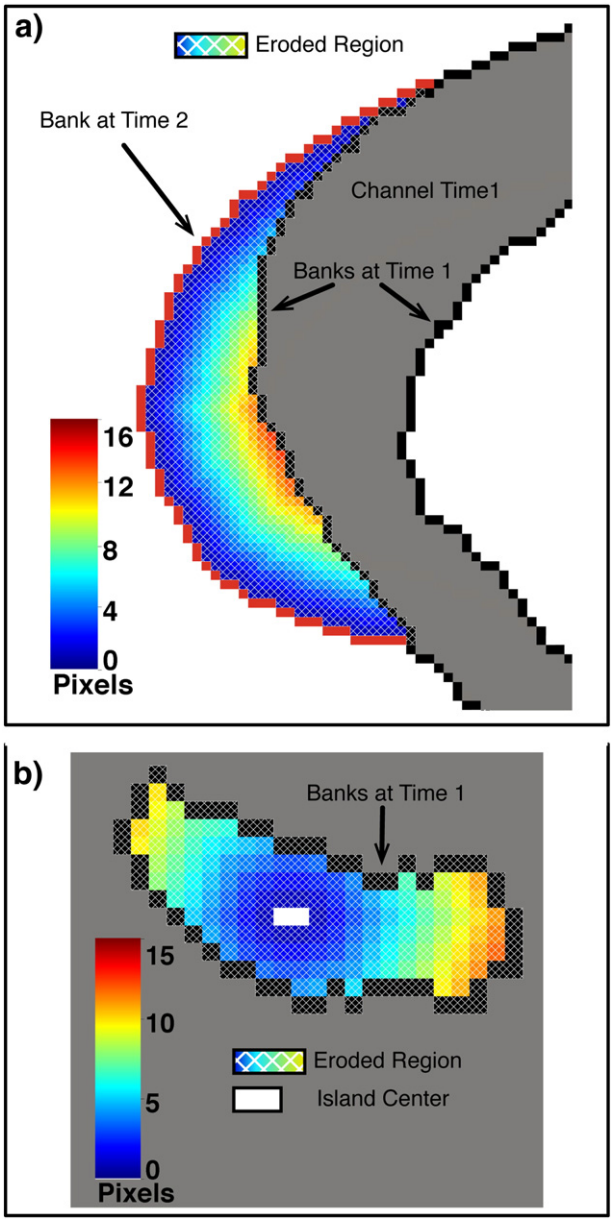

Fig. 3. Graphical illustration of the determination of erosion distances (the method is identical for accretion). a) A distance map (the colored pixels) is generated for each unique bank segment from the Time 2 channel mask (red line) and intersected with the Time 1 bank pixels (black). A linear rate of bank change is calculated by dividing the distance values by the time interval. b) Measurement of erosion distances for an island that completely erodes between Time 1 and Time 2. The distance map is created from the pixel(s) in the interior of the island (white pixel in colored region) that were furthest from any bank on the island perimeter at Time 1. The distances from bank pixels (black) to this interior point are determined by the intersection with the distance map.

or anastomosing channels with islands because our analyses include island margins as banks.

We assign erosion rates to bank pixel locations in the Time 1 raster and accretion to pixels in the Time 2 raster because the reference bank pixels are only present at one time in the case of mid-channel islands that completely erode or form between the two time intervals. In these instances, SCREAM calculates change distances from the banks of the island to the pixel in the interior of the island furthest from any of the bank pixels (Fig. 3b).

2.3. Width and bank aspect

Channel width is commonly measured orthogonal to the mean downstream flow direction, which is assumed to be approximately parallel to the inferred channel centerline (Pavelsky & Smith, 2008; Shields et al., 2000). For a river channel with parallel banks and a uniform width, this width will be the minimum distance between banks on opposite sides of the river. In rivers with complex channel planforms the shortest distance between two banks may significantly differ from the flow-normal cross sectional width (Fig. 4). In order to address complex river planforms, SCREAM uses both distance and bank orientation to determine the channel width perpendicular to the inferred flow direction that is assumed to be parallel to the local bank orientation.

SCREAM sequentially calculates the channel width for each bank pixel in the river mask at each time interval. At each bank pixel (Fig. 4 'target pixel'), SCREAM determines the distance and angle to all the other bank pixels that fall within a subset of the river mask (Fig. 4 'preliminary search window'). Any bank pixel in this window with an angle beyond that of the 'target' bank aspect $\pm 20°$ is eliminated from further consideration (Fig. 4, 'aspect screening window'). We define the bank aspect as the orthogonal to the bank face (parallel to the direction of bank retreat), which ranges from 0 to 359° in accordance with a traditional compass rose where 0° represents north. The bank aspect used to set the screening window is determined by fitting a line to five bank pixels centered on the 'target' pixel (Fig. 4 'preliminary bank orientation'). From this subset of possible matching pixels, SCREAM selects the pixel with the minimum distance from the 'target' pixel, and stores the distance and angle between it and the 'target' pixel as the width and new bank aspect.

2.4. Bank curvature and radius of curvature

The determination of bank aspects at all bank pixels allows for the calculation of the change in bank orientation over user-specified distances along each bank segment. This change in bank orientation divided by distance (radians/L) provides an estimate of bank curvature and its inverse the radius of curvature (L/radians).

SCREAM calculates curvature at the channel banks, rather than along the centerline, using an approach similar to that originally proposed by Nanson and Hickin (1983). This approach calculates curvature over two intervals centered on each bank pixel and then averages the two values. We use default values of two and four local channel widths the length of the intervals, following Nanson and Hickin (1983), but the interval can also be defined by the user if desired. To reduce noise in the curvature values, we first locally smooth the bank aspects using a Savitzky–Golay filter following the approach of Fagherazzi, Gabet, and Furbish (2004). We set the default smoothing coefficients to remove high frequency and low amplitude noise resulting from the non-continuous

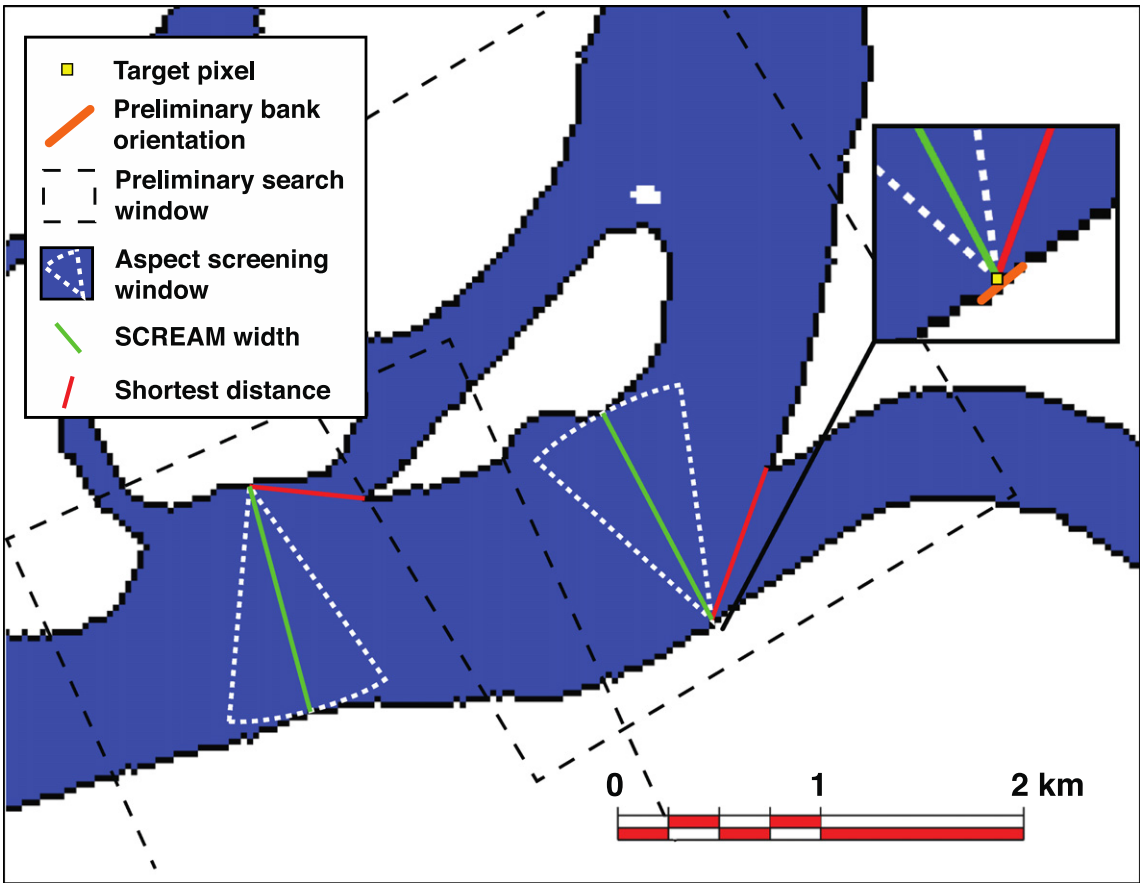

Fig. 4. An illustration of the determination of channel width. The red lines represent the shortest distance from a bank pixel to another bank line; the white dashed lines indicate the 40-degree screening window; and the green lines are the shortest paths in the screening window from a target pixel (yellow) to the other bank.

increments in bank aspects arising from the pixel-based representation of the channel banks. Increasing or decreasing the distance interval over which the curvature is calculated provides the ability to examine the influence of different scales of roughness on bank measurements of bank curvature and how these variations may relate to bank erosion (Darby et al., 2010; Kean & Smith, 2006a, 2006b). The smoothing of the aspect values reduces the noise but still preserves the physical location of the bank pixels, in contrast to methods that smooth the vertices (or pixel locations) of the line prior to calculating the curvature (e.g. Fagherazzi et al., 2004; Güneralp & Rhoads, 2008; Legleiter & Kyriakidis, 2006).

SCREAM also assigns a sign value to each curvature measurement: positive for concave (typically banks on the outside of a bend) and negative for convex (typically banks found on the inside of a bend). SCREAM determines the sign of the curvature by finding the pixel that falls midway along a line connecting the endpoints of the curvature interval and testing whether this midpoint pixel falls inside or outside of the river channel. Segments with midpoints falling in the river are assigned a positive value, indicating a concave bank. Although arbitrary, this sign convention allows for a straightforward evaluation of patterns of erosion and accretion relative to the inside and outside banks of river bends.

2.5. Centerline extraction, channel segmentation, and sinuosity

To provide spatial context to the measurements of channel change, width, and other planview properties, SCREAM can segment the channel at regularly spaced, user-specified, intervals (Fig. 5). The spacing of the segment boundaries uses distances measured along the channel centerline. For single-threaded channels, the centerline falls midway between the outer banks. In a multi-threaded system, the centerline represents the midpoint between the two outermost banks of the larger channel belt similar to the approach taken by the RivWidth program (Pavelsky & Smith, 2008).

Generation of the channel centerline used in the segmentation process uses a distance mask generated from the binary mask of the river channel where all of the islands have been removed so that the

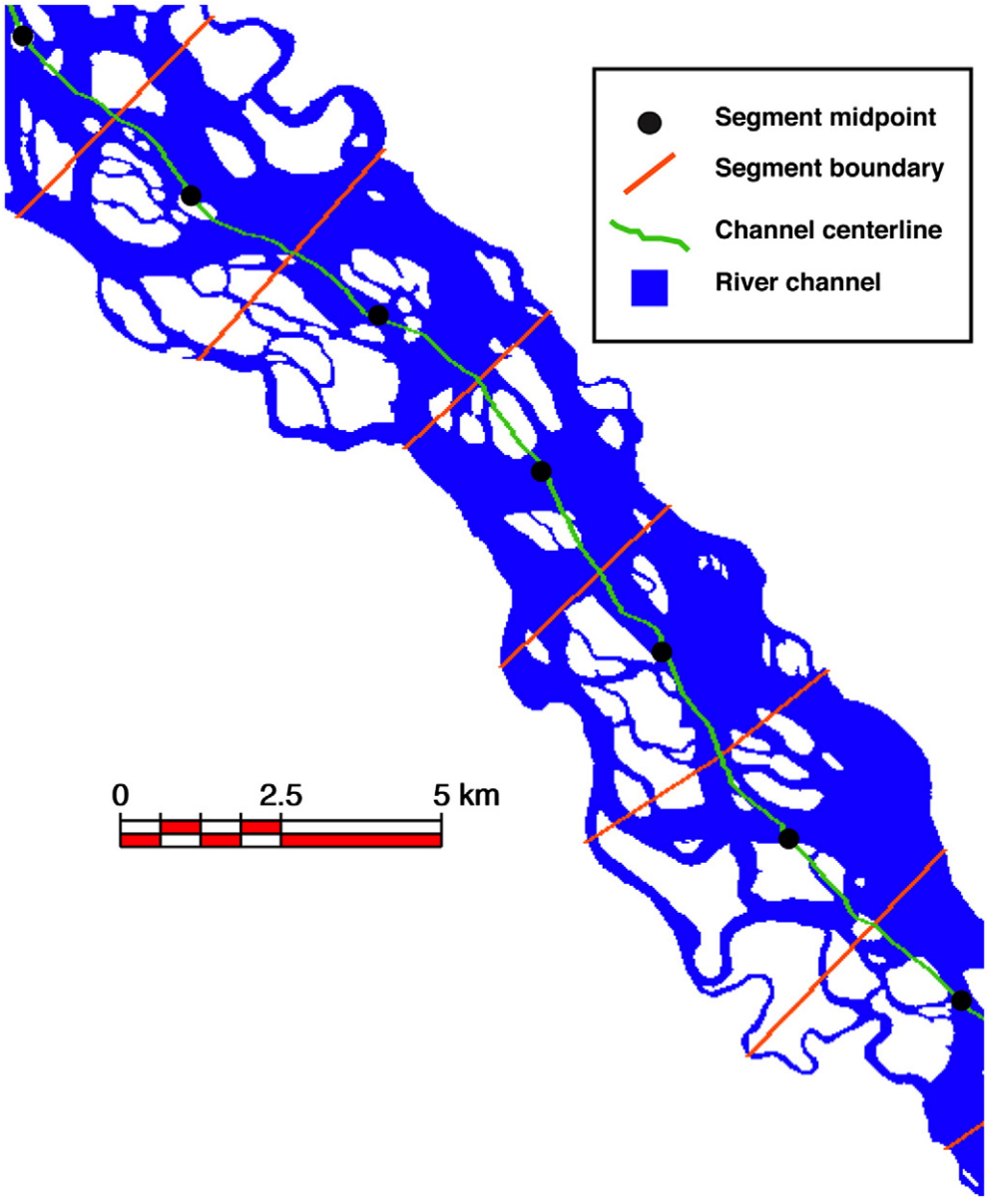

Fig. 5. An example of a portion of the Yukon River binary channel mask showing segmentation boundaries (red) and the centerline along which channel distances were calculated (green). The section boundaries are evenly spaced along the centerline, but do not have equal areas. The black points mark the midpoint of the section on the centerline.

distances are measured from the outermost bank segments. The distances in this mask are analogous to elevations in a digital elevation model (DEM) in which the highest local elevations (found along the middle of the channel mask) form a drainage divide. Prior research used a similar skeletonization process (Fisher et al., 2013; Graham, Reid, & Rice, 2005; Pavelsky & Smith, 2008). In addition to determining unique channel centerlines at Times 1 and 2, SCREAM calculates an average centerline that lies between the two time specific centerlines. This averaged centerline may be used as a common reference for relating the spatial locations of river changes across multiple time periods.

The segmentation algorithm then uses the centerlines for each time interval to divide the river raster into segments of equal length. Due to irregularities in the width between the outermost boundaries in many rivers, these segments commonly do not have equal areas. On some wide multi-threaded rivers with irregular outer boundaries, the use of lines orthogonal to the channel centerline to segment the channel (e.g. Alber & Piégay, 2011; Gangodagamage, Barnes, & Foufoula-Georgiou, 2007; Notebaert & Piégay, 2013; Pavelsky & Smith, 2008) led to intersecting boundary lines that resulted in channel fragments isolated from the centerline. Therefore, as an alternative to centerline orthogonals, SCREAM finds matching pairs of centerline and boundary pixels that are both spaced at regular intervals and segments the channel on lines connecting these pairs. To match a centerline pixel with a boundary pixel SCREAM uses the distance maps of the filled channel and takes a steepest "walk" from the centerline to each boundary. The paths of these steepest walks do not cross (avoiding isolated fragments) but the spacing end points on the boundary may become irregularly spaced in very complex channels. In these instances, if the spacing between adjacent boundary points is less than half the specified segmentation interval SCREAM adjusts the location of the points to be evenly spaced between its neighboring boundary points. SCREAM then segments the channel along straight lines connecting the paired boundary and centerline points. The relative downstream distance and latitude and longitude of the midpoint of each segment is calculated and recorded.

Using this segmentation, the mean, median and standard deviation of erosion/accretion rates, and channel widths may be calculated for each segment along the channel belt. Segmentation also allows for the calculation of the total area of erosion/accretion in each segment. Additionally, SCREAM calculates the total area of water and islands, the total length of all banks and the length of island banks, and the total number of islands in each segment.

SCREAM calculates two measures of width for each segment: 1) the mean of all the widths measured in a segment, and 2) the mean 'cumulative' width of all channel threads in a segment. The 'cumulative' width is calculated by dividing the total area of river channel pixels in the segment by the length of the segment. This metric provides an estimate of the average of combined widths of all channel threads in any finite length of the river. Our cumulative width is functionally equivalent to the "effective" width of Yamazaki et al. (2014), which is calculated by dividing the total area of a segment (water and islands) by a representative width of the segment and is also similar to the approach used by Church and Xu (2015) to calculate reach averaged channel widths.

SCREAM calculates the mean sinuosity for each segment from a continuous estimate of sinuosity at every centerline pixel, using a moving window with a default value of 100 mean channel widths (Snow, 1989). SCREAM calculates sinuosity by dividing the centerline distance by the straightline Euclidian distance between the centerline endpoints within the window. In the case of multi-threaded channels SCREAM reports the sinuosity of the larger channel belt and not the sinuosity of individual channel threads within this belt.

2.6. Output

SCREAM produces two types of output: GeoTiff rasters and text files. Rasters may be output for any of the pixel-based measurements: erosion/accretion rates, width, aspect, and curvature, as well as, for the centerline pixels, associated downstream distance, and the segmented channel. Text files store measurements for every bank pixel as well as for segments along the channel, with measurements referenced to the relative downstream position and latitude and longitude of the segment (Table 1).

3. Results

3.1. SCREAM metrics

SCREAM was tested on several Arctic rivers and a tropical river (Fig. 6) that ranged in width from 70 to 2000 m and varied in planform morphology from single-thread to braided. Historical aerial photographs and satellite imagery with pixel resolutions ranging from 2 to 30 m were used for these analyses. When presented in raster space, the analyses provide a very detailed view of river width, bank aspects, and the spatial patterns of erosion and accretion (Fig. 7), which may be compared at different time intervals for an individual river, used to compare characteristics between river systems, or used to explore relationships between erosion and accretion rates and river geometry. For example, the distribution of channel widths could be used as an indicator of channel type, where a single-threaded river would have a normal distribution of channel widths and a multi-threaded river would have a skewed distribution. Fig. 8 is illustrative of this concept. The largely single-threaded Strickland River, Papua New Guinea has a nearly normal distribution and the complex, multi-threaded Yukon River, Alaska has a highly skewed distribution of widths dominated by a large number of small channels.

The measurement of bank aspects allows a novel view of spatial patterns of change (Fig. 9). On the Yukon River, plots of the distribution of bank aspect (Fig. 9a) and the rates of erosion (Fig. 9b) show that banks facing to the southeast had the lowest distribution, but the highest rates of erosion. Such information has the potential to help identify river systems where thermally controlled processes may be affected by solar radiation and influence erosion rates. These systems include permafrost-dominated rivers and temperate rivers where freeze thaw cycles may result in disaggregation of bank materials and increased net erosion (Lawler, 1986; Leopold, 1973; Pizzuto, 2009; Wolman, 1959; Wynn, Henderson, & Vaughan, 2008; Yumoto, Ogata, Matsuoka, & Matsumoto, 2006). Even in systems not sensitive to thermal dynamics, the analysis of erosion rates by bank aspect may provide insight into the dominant directions of meander migration and growth (Hooke, 1984).

Mean erosion and accretion rates and total area eroded/accreted with distance along a river segment provides a spatial view of variations in river dynamics, facilitates the examination of patterns of change over time, and allows for these changes to be related to sinuosity and other channel planview attributes (e.g., number of islands, size of islands, and overall channel lengths in a segment) in a manner similar to the analysis of the Amazon River by Mertes, Dunne, and Martinelli (1996). For example, Fig. 10 shows erosion rates along the Yukon River between 1986 and 2008. The total erosion and accretion areas can also be compared at discrete intervals along the channel to identify regions of net sediment loss or gain (Fig. 11). Combined with cross-sectional data on the relative heights of eroding banks and accreting bars, this output can be used to calculate the volume of sediment entering or leaving a river section due to the lateral movement of the channel (Church, 2006; Lauer & Parker, 2008a). Erosion rates can also be scaled using measurements of channel width and radius of curvature Hooke (1980), allowing comparison of rates along a river and between river systems of vastly different sizes and channel morphologies. The ability to examine the relationship between erosion rates and channel curvature at all bank pixels represents a significant opportunity to expand current datasets and rigorously test the control of curvature on bank erosion rates.

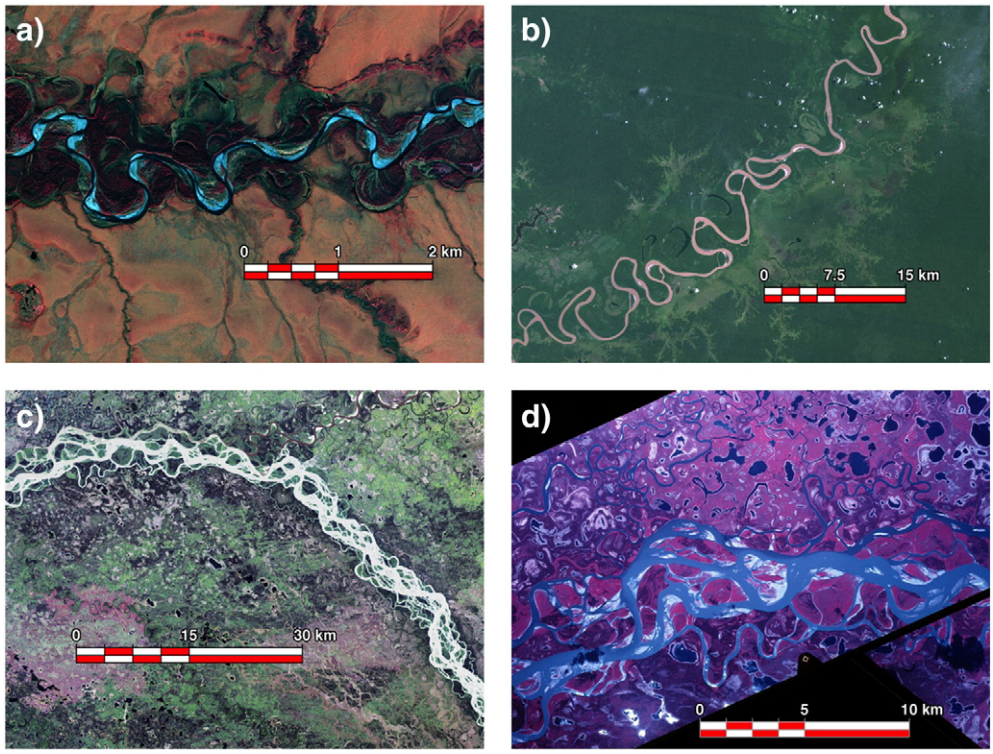

Fig. 6. Images of portions of the river channels analyzed by SCREAM: a) the Selawik River in northwest Alaska (September 24, 2009 Geoeye 2 m false color image (near infrared, red, and green bands)); b) the Strickland River, Papua New Guinea (March 26, 1993 Landsat 5 30 m natural color (Bands 3, 2, and 1), path 65, row 99); c) the Yukon River, Alaska (August 23, 2008 Landsat 5 30 m natural color composite (Bands 3, 2, and 1), path 69, row 13) at 30 m/pixel resolution (image id: L5069013_01320080823); and d) the Yukon River (1974 color infrared aerial photograph scanned with a 2.5 m/pixel resolution).

SCREAM output allows for the examination of downstream trends in channel width with two metrics: the average channel width within a segment of the channel belt; and the mean cumulative width of all of the channel threads within a segment of the river (Fig. 12). For a single-threaded channel, the average width provides a measure of downstream trends in channel width with less noise than measurements extracted from regularly spaced cross sections. The mean cumulative width represents a potentially more useful estimate of the effective channel cross-section of multi-threaded channels for hydrological modeling purposes (Allen & Pavelsky, 2015; Pavelsky & Smith, 2008; Yamazaki et al., 2014), because the presence of large numbers of relatively small channels (Fig. 8) will result in average widths significantly less than the average cumulative width of all of the channels in a segment.

3.2. SCREAM measurement errors

We quantified the error in measurements of erosion, local channel width, and bank aspects to assess the accuracy of the metrics generated by SCREAM. It was assumed that the error in accretion and erosion rates would be the same because they employed identical measurement methodologies. Errors in river planview properties and change may arise in each step of the image analysis and change detection process: image registration, feature classification/extraction, and analysis of the binary rasters. These errors must be accounted for and quantified (Downward, Gurnell, & Brookes, 1994), in order to have confidence that documented change in river systems are not artifacts of the analysis. Mount, Louis, Teeuw, Zukowskyj, and Stott (2003) provided a detailed methodology for quantifying the errors associated with measurements of channel bankfull width from sequences of aerial photography, and Mount and Louis (2005) explained how to propagate errors from bankline delineation into measurements of centerline migration rates. In these analyses, the source of error falls into two categories: 1) image registration, and 2) feature identification and extraction. Errors can also arise during the generation of the binary channel masks required by our analysis, but we do not attempt to quantify this error because these masks may be generated by a number of different techniques. Instead, we only quantify error arising from our methodology and the application of SCREAM to these masks. The propagation of errors arising from image registration and feature identification into metrics generated by SCREAM is discussed in Section 4 and in the Supplementary data.

Although image resolution will dictate whether a riverbank can be delineated (Congalton & Green, 2008), the ability to accurately measure erosion, accretion and width is a function of the size of the river being analyzed, rate of the channel change, and the time interval between images (Grabowski, Surian, & Gurnell, 2014; Mount et al., 2003). For example, images with high spatial resolution would be needed to accurately measure small shifts in a slowly changing river over a short time interval, but large shifts that are greater than the error in delineating the boundaries of the same river could be detected with coarser-resolution imagery with longer time periods between images.

Ideally, quantification of error would be based on the comparison of the SCREAM results to a set of independently obtained ground-truthed values, but measurements of erosion were not available for the time periods of images. Additionally, a field-based assessment of measurement errors would require a subtraction of image registration and classification errors from the total error in order to isolate the fraction of the error associated with the SCREAM analysis. Therefore, our error assessment was performed by comparing SCREAM-generated results against manual measurements made using the measurement tool in a GIS software package at a number of randomly selected locations along the river channels. The same analyst performed a duplicate set of width and erosion measurements on the most complex river system on which SCREAM was tested (the Yukon River) in order to quantify the human errors of interpretation and precision inherent in these manually measured values. We believe these manual comparisons to be a conservative estimate because they reduce judgment errors associated with

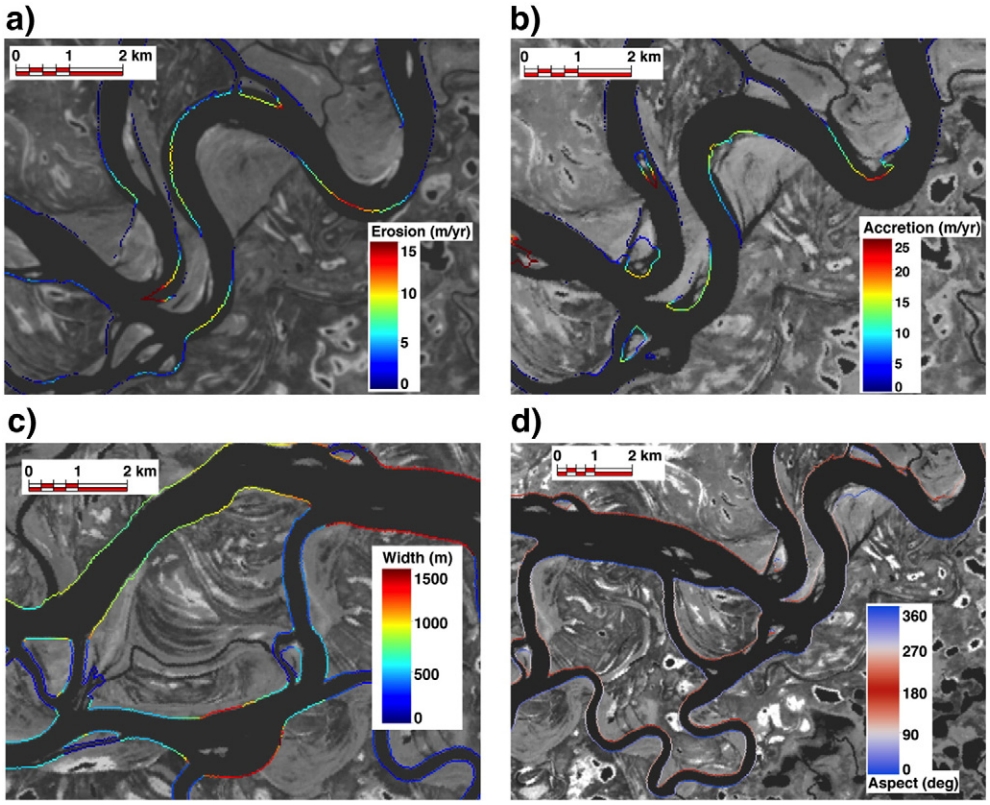

Fig. 7. Raster-based output from SCREAM. a) Bank pixels showing erosion rates between 1986 and 2008 of a small portion of the Yukon River. The bank pixel locations correspond to the channel banks in 1986 and the underlying panchromatic image was collected in 2008 by Landsat 5. b) Accretion rates between 1986 and 2008 shown at the 2008 bank locations in scaled colors overlain on the panchromatic image. c) Local channel widths for all 1986 bank pixels. d) Aspects of the banks in 1986. Discharge measured at the Stevens Village gauge 90 km downstream (USGS ID: 15453500) was 10,250 cubic meters per second (cms) on June 15, 1986 and 6230 cms on August 30, 2008. The Landsat images were collected on June 15, 1986 (path 70, row 13) for panels b–d and August 20, 2008 (path 70, row 13) for panel a.

different analysts when there is ambiguity in deciding the correct measurement. Between 100 and 250 pixel locations were selected from each of three river systems that varied both in size and planform morphology in order to measure local channel width, bank erosion, and aspect. The imagery used for these systems ranged in resolution from 2 to 30 m/pixel.

Table 2 presents a summary of error assessments for SCREAM analyses; the erosion values are linear distances in meters, not rates. A

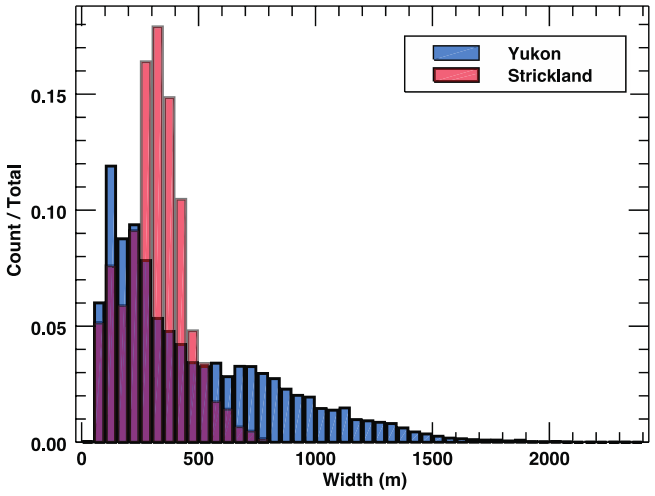

Fig. 8. Histograms of local channel widths generated from the 1986 mask of the Yukon River and the 1993 channel mask of the Strickland River.

Wilcoxon rank sum test was performed to test whether each set of SCREAM-derived values and corresponding manual measurements were from continuous distributions with equal medians (Zar, 1999), because the distributions of many of the measurement sets were right skewed and non-normal. The Wilcoxon tests only rejected the null hypothesis for the cumulative widths for the Strickland River, indicating that all of the manual and SCREAM-derived measurements were comparable except in this isolated case.

We also calculated a Nash–Sutcliffe efficiency coefficient (Nash & Sutcliffe, 1970) for each set of measurements (Table 2). The efficiency coefficient was developed for hydrological modeling and results in values ranging from $-\infty$ to 1, where a value of 1 indicates a perfect agreement between model predictions and observed data. Nash–Sutcliffe coefficients of efficiency for all measurements, excluding the cumulative widths, were >0.63, with 9 of the 13 comparisons having values >0.95, suggesting that SCREAM-generated measurements agree well with those made manually.

Finally, for each set of measurements, we report the standard error (SE) of the root mean square error (RMSE) of the differences between the two methods, because the SE is a more appropriate measure than the RMSE for evaluating and propagating errors in river change studies, although it is less conservative (Mount & Louis, 2005). Quantitatively, the SEs confirm that the measurement errors associated with our analysis were low. SEs for erosion distance ranged from 0.06 to 1.2 m (0.02 to 0.6 pixels), while SEs in local width ranged from 1.4 to 12.1 m (0.05 to 1.4 pixels). The larger errors associated with the width measurements do not increase with the magnitude of the measurements; there was a very weak relationship, at most, between the magnitude of the measurement and the size of the error, suggesting that the error in these measurements may be propagated as a fixed value rather than as a

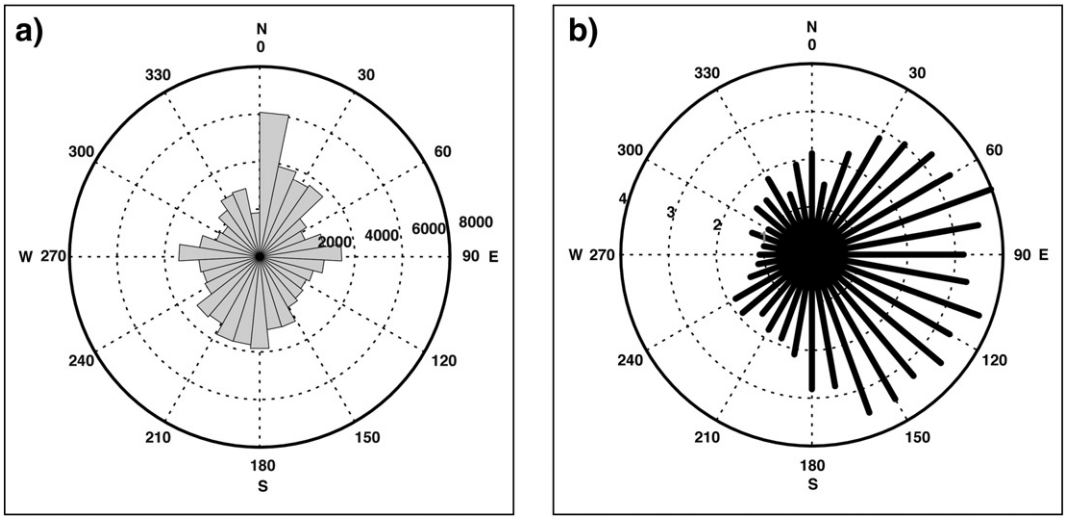

Fig. 9. a) The distribution of all bank aspects for the 1986 mask of the Yukon River. The dashed circles indicate the count of bank aspects within each aspect bin. b) Mean erosion rates by bank aspect binned in 10 degree increments. The erosion rates were determined based on changes in the river between 1986 and 1994. The dashed inner circles indicate erosion rates ranging from 0 to 4 m/yr.

percent of the measurement itself. SE values for the manual measurements on the Yukon River (1986–2008) were within 30% of those for SCREAM, suggesting that a significant portion of the SCREAM errors may arise from the inherent uncertainty in the manual measurement methodology. Overall, the low standard errors, the results of the statistical tests, and the errors associated with the manual measurements all indicate that SCREAM-generated width and erosion measurements do not differ significantly from those obtained by manual measurements.

Low SEs of measurements of bank aspects (0.64 to 1.7°) on the Yukon (1986–2008), Selawik, and Strickland Rivers suggest that SCREAM does well at measuring the riverbank orientation. Manual evaluation of curvature and radius of curvature proved more challenging and could only be performed in a qualitative manner. Radii determined by drawing circles superimposed onto channel bends (Lagasse, Spitz, Zevenbergen, & Zachmann, 2004) gave values consistent with the range calculated by SCREAM. The placement and fit of circles, however, can be quite subjective in general (Hooke, 1984), and has been noted to be problematic on compound and sharp bends (Hooke & Yorke, 2010). Section 4 presents a comparison of SCREAM's curvature values with the algorithms developed by Legleiter and Kyriakidis (2006).

Manual measurements of the cumulative width on a multi-threaded river would require an analyst to measure each individual channel width and then sum these widths along a cross section that bisects the network of channels. Obtaining enough cumulative measurements to calculate a robust average width along a section can be very labor intensive and time consuming. Due to this limitation we only evaluated cumulative widths on single-threaded sections of rivers and a simple synthetic multi-thread channel that had straight segments with 1 to 4 channels of varying sizes.

Of the river systems tested, the Strickland and Selawik rivers had large numbers of segments with only one channel thread, 284 out of 428 and 219 out of 422, respectively. The SEs in cumulative width for both systems was low: 1.38 m (0.05 pixels) for the Strickland and 0.85 m (0.42 pixels) for the Selawik. These errors, however, were not randomly distributed. The cumulative width was systematically smaller than the mean width by 6 to 7% which appears to have resulted from an overestimation of segment length when distances were calculated along the pixel-based delineation of the segment's centerline. Despite accounting for the difference in distance between diagonally ($\sqrt{2}$) and orthogonally (1) connected pixels, centerline distances typically varied

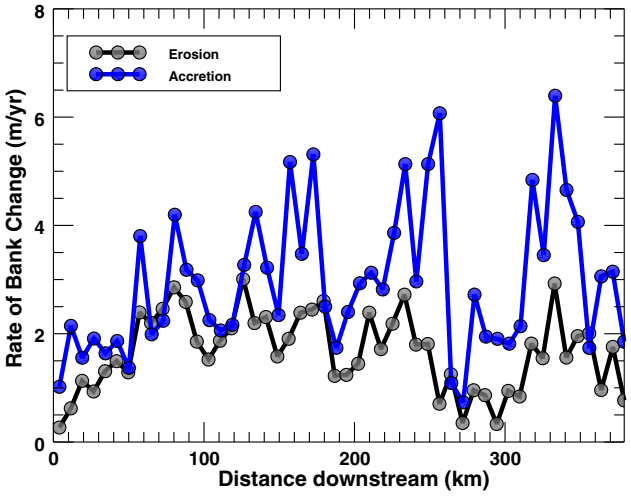

Fig. 10. Erosion (a) and accretion (b) rates averaged at regularly spaced intervals along the Yukon River for the time period of 1986 to 2008.

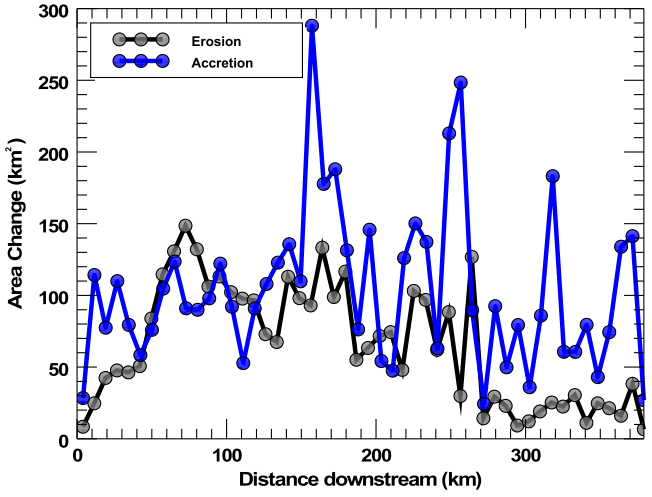

Fig. 11. Total area of eroded and accreted floodplain for a portion of the Yukon River between 1986 and 2008. The areas of accretion exceed erosion for a large portion of the reach, an imbalance that reflects the infilling of the several large oxbows.

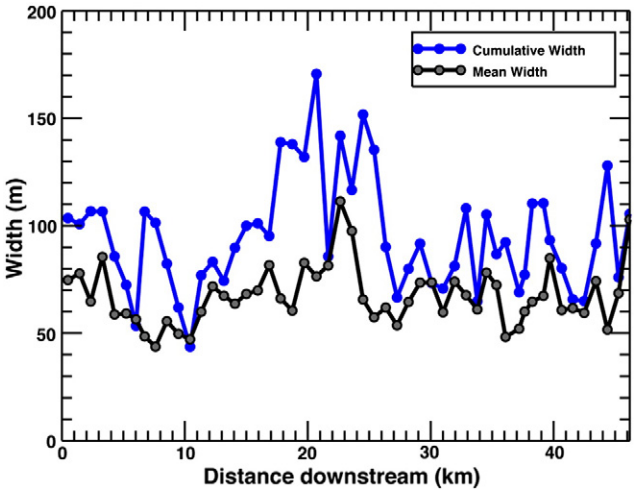

Fig. 12. Measured widths for a portion of the Selawik River, Alaska from a 1981 aerial photograph-derived channel mask. The mean channel width calculated at evenly spaced intervals is shown in black and the average cumulative channel width of each segment is displayed in blue. Where there is only a single channel thread in a segment the mean and cumulative widths are equal.

from manually measured distances by ~6%; an error consistent with those reported from other studies calculating streamline distances from raster-based data (da Paz, Collischonn, Risso, & Mendes, 2008; Paz & Collischonn, 2007).

3.3. Comparison of methodologies

The large diversity of methodologies for quantifying river planview change and characteristics renders comparison of metrics between studies challenging, because each was developed for different applications and is reported in different formats (Table 1). Rather than judge the relative accuracy or utility of one method over another, we provide a comparison of rate of bank erosion inferred from lateral migration made by PST (ArcGIS-based Planform Statistics Toolbox (Aalto et al., 2008), available at: http://www.nced.umn.edu/content/stream-restoration-toolbox), measurements of bank curvature using the Legleiter curvature code (LCC; Legleiter and Kyriakidis, 2006), and mean cumulative width calculated by RivWidth (Pavelsky & Smith, 2008) to comparable measurements using SCREAM. A natural river channel with a range of planform patterns was used for the analysis of mean cumulative width, while a simple synthetic single-threaded test channel was created with a periodic function with constant width (Fig. **13**) to assess the rate of bank erosion and bank curvature because each methodology had a different measurement technique that could not be readily compared on a natural system.

3.3.1. Rate of bank erosion

PST does not directly measure rate of bank erosion; it measures channel migration rates, which can be used to infer rates of bank erosion in the controlled case of our test channel. Specifically, erosion and accretion are equal along the channel and match centerline migration (refer to Figs. 1a and 13). PST derives representative centerlines for two time intervals from vector-based representations of channel banks, and determines centerline migration by measuring the displacement in the location of the centerlines.

We applied the PST to the test channel and recorded migration rates at intervals of 25 m and 100 m intervals along the channel and plotted them against 100 m averages of the continuous SCREAM erosion measurements (Fig. 14). A direct one to one comparison of rates between the two methods was not possible because PST provides discrete measurements at fixed intervals along the centerline while SCREAM's values represent the average erosion rate of all the bank locations within each 100 m long interval. In instances where channel migration directly reflects bank erosion, SCREAM's bank erosion rates appear to be directly

Table 2
Summary of error quantification.

River (dates)	Measurement	Image resolution (m/pixel)	Mean erosion (m)	Max erosion (m)	Mean width (m)	Max width (m)	*n*	Wilcoxon[a]	*p*[b]	Nash–Sutcliffe EC[c]	SE of RMSE[d]	SE (pix)
Yukon		30	39	932	482	2327	–	–	–	–	–	–
(1986–2008)	Erosion (m)	–	–	–	–	–	250	N	0.86	0.99	0.67	0.02
	Local width (m)	–	–	–	–	–	250	N	0.85	0.76	12.14	0.4
	Aspect (deg)	–	–	–	–	–	250	N	0.77	0.96	1.27	NA
Yukon	Comparison of manual	30	–	–	–	–	–	–	–	–	–	–
(1986–2008)	measurements											
	Erosion (m)	–	–	–	–	–	250	N	0.68	0.99	0.52	0.02
	Local width (m)	–	–	–	–	–	250	N	0.82	0.87	8.89	0.30
Yukon		2.5	18	543	354	2077	–	–	–	–	–	–
(1974–1981)	Erosion (m)	–	–	–	–	–	195	N	0.89	1.00	0.06	0.03
	Local width (m)	–	–	–	–	–	195	N	0.98	0.98	3.57	1.40
Selawik		2.0	21	160	66	316	–	–	–	–	–	–
(1981–2009)	Erosion (m)	–	–	–	–	–	100	N	0.75	0.63	1.2	0.6
	Local width (m)	–	–	–	–	–	100	N	0.97	0.93	1.44	0.72
	Cumulative width (m)	–	–	–	–	–	219	N	0.86	0.06	0.85	0.42
	Aspect (deg)	–	–	–	–	–	82	N	0.84	0.98	1.7	NA
Strickland		30	57.4	636	336	826	–	–	–	–	–	–
(1993–2007)	Erosion (m)	–	–	–	–	–	100	N	0.97	0.99	0.65	0.02
	Local width (m)	–	–	–	–	–	100	N	0.69	0.98	1.61	0.05
	Cumulative width (m)	–	–	–	–	–	284	Y	$<1e^{-4}$	0.86	1.38	0.05
	Aspect (deg)	–	–	–	–	–	100	N	0.74	0.99	0.64	NA
All systems	Erosion (pix)	–	–	–	–	–	645	N	0.93	0.86	–	0.09
(pixels)	Local width (pix)	–	–	–	–	–	645	N	0.98	0.99	–	0.47

Notes: all erosion values are linear distances, not rates.
n — number of measurements in error assessment.
[a] Wilcoxon rank sum test, reject null hypothesis at 5% significance (N — no, Y — Yes).
[b] *p*-Value for Wilcoxon test.
[c] Efficiency coefficient.
[d] Standard error (SE) of root mean square error (RMSE).

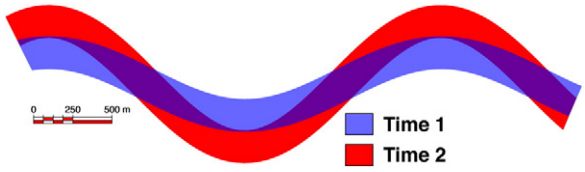

Fig. 13. Synthetic river channel generated using a periodic function with constant width.

comparable to migration rates determined using PST's centerline-based methodology (Fig. 14).

3.3.2. Bank curvature

We evaluated SCREAM's estimates of bank curvature by comparing curvature from the upper bank in the Time 1 synthetic channel (Fig. 13) to curvatures calculated from the second derivative of a spline generated from a digitized line segment (Fagherazzi et al., 2004; Güneralp & Rhoads, 2008; Legleiter & Kyriakidis, 2006) as represented by LCC. In its creation of a spline, LCC produces spatial values that are not directly comparable to raster locations, requiring a transformation of the LCC curvature values into raster-space by performing a piecewise linear interpolation of endpoints, curvature maximums, and zero crossing points matched to the SCREAM output. Fig. 15a compares SCREAM curvatures calculated over bank distance intervals of 4, 2, and 1/2 channel widths to bank curvature calculated using the LCC smoothed 5 times with a 1-channel width wide filtering window and fit with a 3rd order polynomial. As the length of the interval over which SCREAM calculates the curvature decreases, the peak SCREAM curvature values approach the LCC-based values (Fig. 15b). Even though the LCC method allows for variation in the size of the smoothing window, the method always determines curvature over an infinitely small distance.

3.3.3. Mean cumulative width

Assessment of error in mean cumulative width for sections of a single-threaded river channel is straightforward (Section 3.2), however, the mean width and the cumulative width of channel segments will not be equivalent at any point along a multi-threaded river. To our knowledge, RivWidth is the only other published methodology (Pavelsky & Smith, 2008) that measures the total width of all channel segments in multi-threaded river systems.

The RivWidth methodology (Pavelsky & Smith, 2008) provides a measure of channel width for both single- and multi-threaded rivers using raster-based binary river masks by determining orthogonals to the channel centerline and counts the number of river pixels that fall on each orthogonal. Assessments performed by Pavelsky and Smith (2008) and our own application of the code suggest that RivWidth provides accurate measurements of width for single-thread systems and where the individual segments of multi-threaded river run parallel to the specified centerline. In systems with non-parallel channel threads, however, the centerline orthogonal may cross the channel segments at oblique angles resulting in an overestimate of the actual channel width. To provide a comparison of SCREAM and RivWidth (version 4), we ran both on a section of the Strickland River in Papua New Guinea that encompasses single- and multi-threaded channels using the SCREAM-generated segments of the river to average RivWidth output over the same regions of the channel. For narrower, single-thread reaches SCREAM and RivWidth estimates agreed closely (Fig. 16a), but diverged somewhat at wider, multi-threaded reaches, but the difference between the two types of channels was not significantly different. The segment with the greatest discrepancy (SCREAM ~1500 m vs. RivWidth ~750 m) had an irregular shape that had a short centerline relative to the total area of the segment resulting in an over-estimate of the width by SCREAM (Fig. 16b). In several reaches where RivWidth estimates exceeded SCREAM measurements (points below regression line), individual channel threads ran sub-parallel to the centerline and the RivWidth orthogonals crossed channel threads at oblique angles resulting in overestimates of widths (Fig. 16c).

4. Discussion

Most existing river analysis methods rely on vector-based representations of river channels for input data. SCREAM, along with RivWidth (Pavelsky & Smith, 2008) and ChanGeom (Fisher et al., 2013) are unique in the use of raster-based channel masks for input and analysis. Even though processing vector-based inputs could reduce computational memory requirements associated with raster-based inputs, SCREAM retains the original raster format of the data throughout the analysis, which is advantageous for several reasons. First, the conversion of raster masks, output from feature extraction software, into vector-based representations of channels has the potential to introduce additional sources of error (Congalton, 1997). Second, in several of the SCREAM analysis routines, the ability to perform computational operations on matrices (rasters) increases the efficiency and significantly reduces the number of operations ("for" loops) required. An evaluation of the performance efficiency of SCREAM relative to raster size and channel complexity is presented in Supplementary data Section 1. Third, our original motivation for quantifying river planview change was largely driven by questions of bank erosion dynamics, rather than river channel migration. As such, we adopted a bank-centric approach that allowed an improved ability to examine rates and patterns of bank change due to

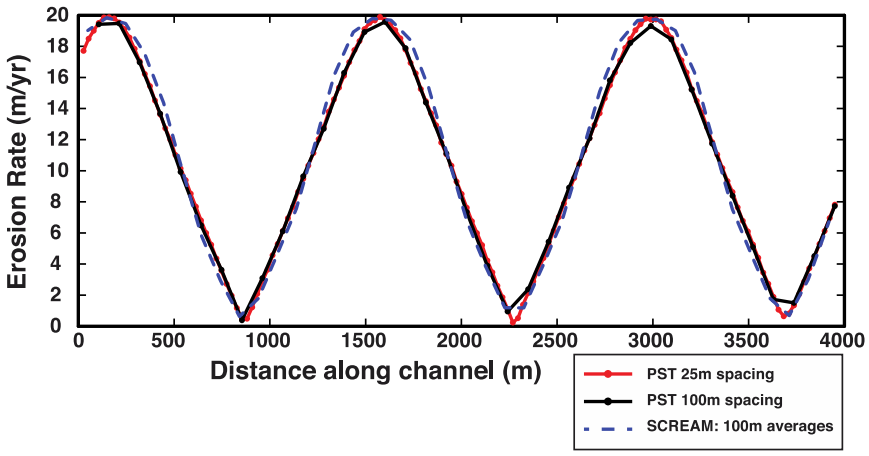

Fig. 14. A comparison of SCREAM erosion rates for a synthetic channel (Fig. 13) averaged over 100 m long segments (blue line) against lateral migration rates determined using the Planform Statistics Toolbox (Aalto et al., 2008) calculated at evenly spaced intervals of 25 (red line) and 100 m (black line) along the channel.

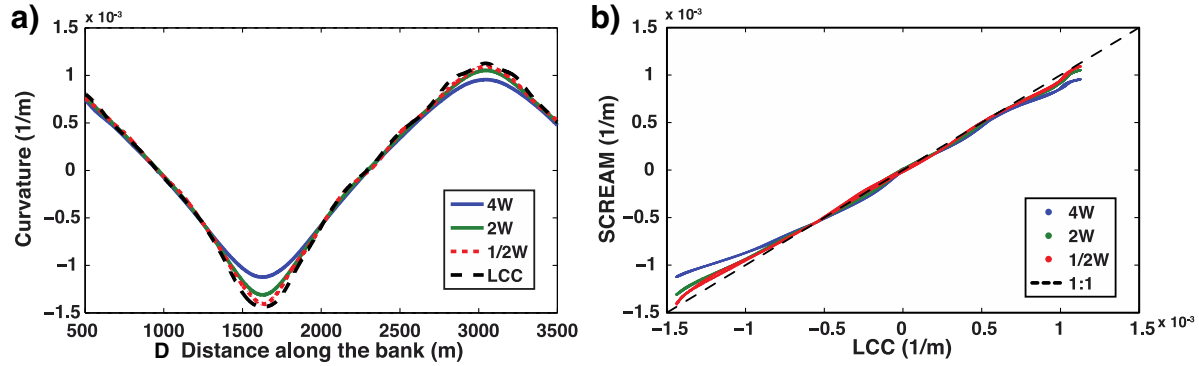

Fig. 15. Comparison of bank curvature values from SCREAM to curvature determined using LCC (Legleiter & Kyriakidis, 2006). The comparison was performed on the top bank in the Time 1 synthetic raster (Fig. 13). a) The black lines show the curvature values obtained using smoothed data, LCC, and a 3rd order polynomial to fit a line to the bank pixels and the data was smoothed 5 times prior to fitting the polynomial. The SCREAM calculated curvature values were obtained using distance intervals of 1/2, 2, and 4 channel widths (red, green, and blue lines respectively). b) A scatter plot showing SCREAM bank curvature values versus the LCC-derived values. The dashed line shows where a 1:1 correlation of values would fall on the plot. As the interval over which SCREAM calculates curvature decreases the values approach those calculated by the LCC method.

the retention of the native pixel resolution of the source imagery. By operating in raster space, SCREAM also provides a very detailed view of river width, bank aspects, and the spatial patterns of erosion and accretion rates (Fig. 7), allowing direct comparison of patterns of bank change to other spatially distributed datasets such as vegetation, permafrost, or sedimentology of the floodplain. Moreover, extracting measurements at every bank pixel in an input raster generates a very large number of unique measurements to support spatial statistical analysis of river erosion/accretion rates, widths, and bank aspects. These attributes may be compared at different time intervals for an individual river, used to compare characteristics between river systems, or used to explore relationships between erosion and accretion rates and river geometry.

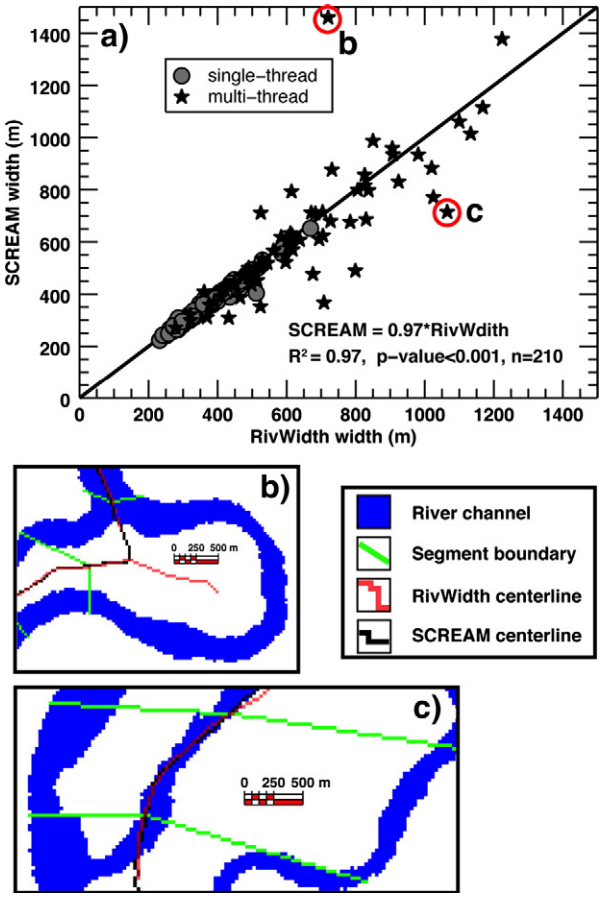

Fig. 16. A comparison of average cumulative widths (by segment) for a portion of the Strickland River, Papua New Guinea, using both SCREAM and RivWidth (Pavelsky & Smith, 2008). a) The slope (0.97) and strong fit ($R^2 = 0.97$, p-value < 0.001) indicate no significant difference between the two methods, but the plot suggests greater ability to measure width for single-threaded channels (filled circles) than for multi-threaded channels (stars). Although channel complexity was not statistically significant, regression analysis (b) indicates that the methods diverge for complex channels as width increases. Panels b and c show segments of the river where the SCREAM and RivWidth measurements provide differing width measurements.

In the process of developing SCREAM we have applied and tested it against a broad range of planform channel morphologies from the simple single-threaded uniform width benchmark channel to the highly complex multi-threaded Yukon River. In all but one test case, the standard error in the SCREAM output, relative to manual measurements, was a fraction of the pixel size of the imagery. We examined the relationship between the errors in width as a function of the size of the width measurement and did not find a relationship. Instead the magnitude of the width errors appears to be related to the complexity of the channel geometry with higher errors occurring for the multi-threaded Yukon River relative to the largely single-threaded Selawik and Strickland Rivers. It appears that this increase in error with channel complexity results from the greater number of islands and a more complex spatial pattern of bank pixels.

The ability to examine the relationship between erosion rates and channel curvature at all bank pixels represents a significant opportunity to expand current datasets and rigorously test the control of curvature on bank erosion rates—bend curvature has been linked to bank erosion (Begin, 1986; Hickin, 1974; Hickin & Nanson, 1975; Hooke & Yorke, 2010; Nanson & Hickin, 1986), while other studies have not found a clear relationship (Beeson & Doyle, 1995). Hooke (1980) suggested that normalizing erosion rates by channel width allows for the examination of the relative influence of other factors, such as bank materials, on erosion rates. Plotting width-normalized erosion rates against width-normalized radii of curvature offers the potential to resolve discrepancies in this relationship.

The SCREAM sign convention for curvature allows for erosion and accretion patterns to be assessed both by the magnitude of the curvature and location inside or outside of channel bends. It is commonly assumed that erosion occurs on outer concave banks and accretion occurs on inner convex banks (Hickin & Nanson, 1984; Wolman & Leopold, 1957), however, several studies have documented that banks with high curvature and flow separation can result in outer bank accretion creating concave bench deposits (Blanckaert et al., 2013; Nanson & Page, 1983; Nanson, 2010; Vietz, Rutherfurd, Stewardson, & Finlayson,

Table 3
Incorporation of misregistration and classification errors.

SCREAM measurement	Misregistration	Classification	Error incorporation
Linear rate of bank change	✔	✔	Error propagation of sums and differences, added in quadrature
Areas of channel change	✓	✓	Supplementary data Sections 2 & 3
Channel width	–	✓	Error propagation of sums and differences, added in quadrature
Cumulative channel width	–	✓	Supplementary data Sections 3
Area of islands	–	✓	Supplementary data Sections 3
Bank aspects	–	–	Not applicable
Bank curvature	–	–	Not applicable
Sinuosity	–	–	Not applicable

2012; Woodyer, 1975). SCREAM-generated data provides a tool for a more detailed examination of these dynamics and variability in erosion patterns across a wide variety of river systems.

Section 3.2 presented the results of our error assessment of the SCREAM's measurements relative to manual measurements of the same metrics. However, to accurately assess the result of measurements derived from remotely sensed imagery, it is also necessary to account for the impact of image misregistration and classification errors. Table 3 provides a summary of the SCREAM measurements impacted by either or both misregistration and classification errors. We do not list measurements made on a single image, such as width, as affected by misregistration because we assume that the relative location between pixels within a single image is accurate. This assumption may not hold in instances where georectification errors result in local distortions at scales less than a channel width. However, in many of our study sites we do not have sufficient, or any independent ground control points, to assess the absolute accuracy of a single image. Therefore, we limited our misregistration error assessment to the relative accuracy of one image compared to another based on the location of common features identifiable in each image in the time series being studied.

Standard error propagation methods are sufficient to assess how linear errors, such as pixel displacement due to misregistration or uncertainty in the location of a river boundary due to misclassification, impact SCREAM-generated metrics of width and erosion/accretion rates. A detailed description of how such errors may be propagated into measurements of channel width and change in positions of centerlines was provided in Mount et al. (2003) and Mount and Louis (2005) and therefore is not repeated here. Determination of how misregistration and classification errors affect area-based measurements of change, however, is a much more complex challenge. A number of studies have examined the effect of misregistration on land cover classification and change detection (Dai & Khorram, 1998; Serra et al., 2003; Van Niel, McVicar, Li, Gallant, & Yang, 2008; Verbyla & Boles, 2000; Wang & Ellis, 2005) and found that small misregistration errors may result in large classification errors particularly as the number of classes and image heterogeneity increases (Verbyla & Boles, 2000; Wang & Ellis, 2005). While these prior studies highlighted the potential impact of misregistration errors, we are not aware of any study that provides a method for quantifying the error in change-areas given a known misregistration or classification error. In our examination of the impact of misregistration error on change-areas in the rivers we studied, we found that errors in the measurement of change-areas strongly depends on the size of the section of river being analyzed and the distribution of bank aspects in that section. Our complete analysis on the impact of misregistration and misclassification on change-areas along with a methodology for estimating the associated errors is presented in Supplementary data Section 2. We highlight that classification errors arising from directional biases in the image, such as shadows, may be explicitly accounted for in SCREAM output since each bank has a recorded aspect. Finally, we discovered a systematic error in measurements that was inherent to measuring distances in a raster-based system. Correcting for this discrepancy represents an area of future improvement and may be solved using Distance Transforms to better estimate actual streamline distances (Butt & Maragos, 1998; da Paz et al., 2008; de Smith, 2004; Paz & Collischonn, 2007).

5. Conclusion

The majority of methodologies developed to quantify planview river properties using remotely sensed imagery have been developed for and applied to single-thread rivers (Table 1). Quantification of the planview dynamics of single-thread rivers has commonly relied on analysis of changes in the location of river channel centerlines between successive images. SCREAM differs from most prior methods in its applicability to characterize rivers with both single and multi-threaded planform morphologies, and it uses a bank-based reference frame for quantifying planview properties and change. The utility of this reference frame in analyzing change in complex channel systems and its provision for a detailed examination of spatial patterns of change and planview properties offers significant opportunities to gain new insights into river dynamics from as fine of a scale as an individual bank pixel to 100 s and 1000 s km of a river. SCREAM provides metrics related to both the planview attributes and dynamics of river systems (Table 1). This suite of metrics allows for a detailed examination of individual rivers and for comparing SCREAM-generated results to a broad range of prior studies using alternative methodologies. For example, our comparison with other methodologies suggests that for single-threaded rivers with a stable width, SCREAM-generated rates of linear bank erosion can be accurately compared to lateral migration rates derived from methods measuring change in the lateral position of channel centerlines. Additionally, SCREAM provides area-based measurements of change for comparison to similar prior studies (e.g. Peixoto et al., 2009; Rozo et al., 2014). Readily available remotely sensed imagery of the earth's surface, combined with the increasing ease and sophistication of methods for automatically extracting features from imagery represents an opportunity to quantify river dynamics and planview characteristics at global scales over decadal time spans.

Acknowledgements

The Early Career Research, Subsurface Biogeochemical Research, Earth System Modeling, and the Regional and Global Climate Modeling Programs within the U.S. Department of Energy Office of Science, Biological and Environmental Research supported this work. Initial efforts in the development of these analysis methods were also supported by the U.S. Department of Energy through the LANL/LDRD Program. We thank Wes Lauer for sharing the Strickland River results for comparison in the development of our methods and for providing valuable insights on analysis methodologies. We also thank five anonymous reviewers and Tim McVicar for detailed and constructive comments on earlier versions of the manuscript.

Appendix A. Supplementary data

Supplementary data to this article can be found online at http://dx.doi.org/10.1016/j.rse.2016.07.005.

References

Aalto, R., Lauer, J.W., Dietrich, W.E., 2008. Spatial and temporal dynamics of sediment accumulation and exchange along Strickland River floodplains (Papua New Guinea) over decadal-to-centennial timescales. J.Geophys.Res *113*, F01S04.

Alber, A., Piégay, H., 2011. Spatial disaggregation and aggregation procedures for characterizing fluvial features at the network-scale: application to the Rhône basin (France). Geomorphology 125, 343–360.

Allen, G.H., Pavelsky, T.M., 2015. Patterns of river width and surface area revealed by the satellite-derived North American River width data set. Geophys. Res. Lett. 42, 395–402.

Asahi, K., Shimizu, Y., Nelson, J., Parker, G., 2013. Numerical simulation of river meandering with self-evolving banks. Journal of Geophysical Research: Earth Surface 118, 2208–2229.

Ashworth, P.J., Lewin, J., 2012. How do big rivers come to be different? Earth Sci. Rev. 114, 84–107.

Baki, A.B.M., Gan, T.Y., 2012. Riverbank migration and island dynamics of the braided Jamuna River of the Ganges–Brahmaputra basin using multi-temporal Landsat images. Quat. Int. 263, 148–161.

Beeson, C.E., Doyle, P.F., 1995. Comparison of bank erosion at vegetated and non-vegetated channel bends. Water Resour. Bull. 31, 983–990.

Begin, Z.B., 1986. Curvature ratio and rate of river bend migration — update. Journal of Hydraulic Engineering-Asce 112, 904–908.

Blanckaert, K., Kleinhans, M.G., McLelland, S.J., Uijttewaal, W.S., Murphy, B.J., Kruijs, A., Parsons, D.R., Chen, Q., 2013. Flow separation at the inner (convex) and outer (concave) banks of constant-width and widening open-channel bends. Earth Surf. Process. Landf. 38, 696–716.

Brice, J., 1977. Lateral migration of the Middle Sacramento River, California. USGS Water-Resources Investigations 77-43, 51.

Brumby, S.P., Theiler, J., Perkins, S.J., Harvey, N.J., Szymanski, J.J., Bloch, J.J., Mitchell, M., 1999. Investigation of image feature extraction by a genetic algorithm. SPIE's International Symposium on Optical Science, Engineering, and Instrumentation. International Society for Optics and Photonics, pp. 24–31.

Butt, M.A., Maragos, P., 1998. Optimum design of chamfer distance transforms. Image Processing, IEEE Transactions on 7, 1477–1484.

Church, M., 2006. Bed material transport and the morphology of alluvial river channels. Annu. Rev. Earth Planet. Sci. 34, 325–354.

Church, M., Xu, J., 2015. Post-regulation morphological change on Peace River. The Regulation of Peace River: A Case Study for River Management. John Wiley & Sons, Ltd., pp. 141–174.

Congalton, R.G., 1997. Exploring and evaluating the consequences of vector-to-raster and raster-to-vector conversion. Photogramm. Eng. Remote. Sens. 63, 425–434.

Congalton, R.G., Green, K., 2008. Assessing the Accuracy of Remotely Sensed Data: Principles and Practices. CRC press.

Constantine, J.A., Dunne, T., Ahmed, J., Legleiter, C., Lazarus, E.D., 2014. Sediment supply as a driver of river meandering and floodplain evolution in the Amazon Basin. Nat. Geosci. 7, 899–903.

Constantine, C.R., Dunne, T., Hanson, G.J., 2009. Examining the physical meaning of the bank erosion coefficient used in meander migration modeling. Geomorphology 106, 242–252.

Costard, F., Gautier, E., 2008. The Lena River: Hydromorphodynamic Features in a Deep Permafrost Zone. Large Rivers, Geomorphology and Management, pp. 225–233.

Costard, F., Gautier, E., Brunstein, D., Hammadi, J., Fedorov, A., Yang, D., Dupeyrat, L., 2007. Impact of the global warming on the fluvial thermal erosion over the Lena River in Central Siberia. Geophys. Res. Lett. 34, L14501.

da Paz, A.R., Collischonn, W., Risso, A., Mendes, C.A.B., 2008. Errors in river lengths derived from raster digital elevation models. Comput. Geosci. 34, 1584–1596.

Dai, X., Khorram, S., 1998. The effects of image misregistration on the accuracy of remotely sensed change detection. Geoscience and Remote Sensing, IEEE Transactions on 36, 1566–1577.

Darby, S.E., Trieu, H.Q., Carling, P.A., Sarkkula, J., Koponen, J., Kummu, M., Conlan, I., Leyland, J., 2010. A physically based model to predict hydraulic erosion of fine-grained riverbanks: the role of form roughness in limiting erosion. Journal of Geophysical Research: Earth Surface 2003–2012, 115.

de Smith, M.J., 2004. Distance transforms as a new tool in spatial analysis, urban planning, and GIS. Environment and planning B: Planning and design 31, 85–104.

Dey, A., Bhattacharya, R.K., 2013. Monitoring of river center line and width—a study on river Brahmaputra. Journal of the Indian Society of Remote Sensing 1–8.

Dillabaugh, C.R., Niemann, K.O., Richardson, D.E., 2002. Semi-automated extraction of rivers from digital imagery. GeoInformatica 6, 263–284.

Downward, S., Gurnell, A., Brookes, A., 1994. A methodology for quantifying river channel planform change using GIS. IAHS Publications—Series of Proceedings and Reports—International Association of Hydrological Sciences. *224*, pp. 449–456.

Eke, E.C., Czapiga, M., Viparelli, E., Shimizu, Y., Imran, J., Sun, T., Parker, G., 2014a. Coevolution of width and sinuosity in meandering rivers. J. Fluid Mech. 760, 127–174.

Eke, E., Parker, G., Shimizu, Y., 2014b. Numerical modeling of erosional and depositional bank processes in migrating river bends with self-formed width: morphodynamics of bar push and bank pull. Journal of Geophysical Research: Earth Surface 119, 1455–1483.

Fagherazzi, S., Gabet, E.J., Furbish, D.J., 2004. The effect of bidirectional flow on tidal channel planforms. Earth Surf. Process. Landf. 29, 295–309.

Fisher, G.B., Bookhagen, B., Amos, C.B., 2013. Channel planform geometry and slopes from freely available high-spatial resolution imagery and DEM fusion: implications for channel width scalings, erosion proxies, and fluvial signatures in tectonically active landscapes. Geomorphology 194, 46–56.

Gangodagamage, C., Barnes, E., Foufoula-Georgiou, E., 2007. Scaling in river corridor widths depicts organization in valley morphology. Geomorphology 91, 198–215.

Gautier, E., Brunstein, D., Costard, F., Lodina, R., 2003. Fluvial dynamics in a deep permafrost zone: the case of the Middle Lena river (central Siberia). Eighth International Conference on Permafrost, Zurich, pp. 271–275.

Gleason, C.J., Smith, L.C., 2014. Toward global mapping of river discharge using satellite images and at-many-stations hydraulic geometry. Proceedings of the National Academy of Sciences *111*, 4788–4791.

Grabowski, R.C., Surian, N., Gurnell, A.M., 2014. Characterizing geomorphological change to support sustainable river restoration and management. Wiley Interdisciplinary Reviews: Water 1, 483–512.

Graham, D.J., Reid, I., Rice, S.P., 2005. Automated sizing of coarse-grained sediments: image-processing procedures. Math. Geol. 37, 1–28.

Güneralp, İ., Rhoads, B.L., 2008. Continuous characterization of the planform geometry and curvature of meandering rivers. Geogr. Anal. 40, 1–25.

Gurnell, A., 1997a. Adjustments in river channel geometry associated with hydraulic discontinuities across the fluvial-tidal transition of a regulated river. Earth Surf. Process. Landf. 22, 967–985.

Gurnell, A.M., 1997b. Channel change on the River Dee meanders, 1946–1992, from the analysis of air photographs. Regulated Rivers-Research & Management 13, 13–26.

Gurnell, A.M., Downward, S.R., Jones, R., 1994. Channel planform change on the River Dee meanders, 1876–1992. Regulated Rivers-Research & Management 9, 187–204.

Hamilton, S.K., Kellndorfer, J., Lehner, B., Tobler, M., 2007. Remote sensing of floodplain geomorphology as a surrogate for biodiversity in a tropical river system (Madre de Dios, Peru). Geomorphology 89, 23–38.

Hickin, E.J., 1974. Development of meanders in natural river-channels. Am. J. Sci. 274, 414–442.

Hickin, E.J., Nanson, G.C., 1975. The character of channel migration on the Beatton River, northeast British Columbia, Canada. Geol. Soc. Am. Bull. 86, 487–494.

Hickin, E.J., Nanson, G.C., 1984. Lateral migration rates of river bends. J. Hydraul. Eng. 110, 1557–1567.

Hooke, J., 1980. Magnitude and distribution of rates of river bank erosion. Earth surface processes 5, 143–157.

Hooke, J., 1984. Changes in river meanders a review of techniques and results of analyses. Prog. Phys. Geogr. 8, 473–508.

Hooke, J., Harvey, A., 1983. Meander changes in relation to bend morphology and secondary flows. Modern and Ancient Fluvial Systems: Special Publication 6 of the IAS, p. 121.

Hooke, J., Yorke, L., 2010. Rates, distributions and mechanisms of change in meander morphology over decadal timescales, River Dane, UK. Earth Surf. Process. Landf. 35, 1601–1614.

Hossain, M.A., Gan, T.Y., Baki, A.B.M., 2013. Assessing morphological changes of the Ganges River using satellite images. Quat. Int. 304, 142–155.

James, L.A., Hodgson, M.E., Ghoshal, S., Latiolais, M.M., 2012. Geomorphic change detection using historic maps and DEM differencing: the temporal dimension of geospatial analysis. Geomorphology 137, 181–198.

Kean, J.W., Smith, J.D., 2006a. Form drag in rivers due to small-scale natural topographic features: 1. Regular sequences. Journal of Geophysical Research: Earth Surface (2003–2012), 111.

Kean, J.W., Smith, J.D., 2006b. Form drag in rivers due to small-scale natural topographic features: 2. Irregular sequences. Journal of Geophysical Research: Earth Surface *(2003-2012)*, 111.

Knighton, D., 1998. Fluvial Forms and Processes: A New Perspective. Arnold, Hodder Headline, PLC.

Konrad, C., Berge, H., Fuerstenberg, R., Steff, K., Olsen, T., Guyenet, J., 2011. Channel dynamics in the Middle Green River, Washington, from 1936 to 2002. Northwest Science 85, 1–14.

Lagasse, P.F., Spitz, W.J., Zevenbergen, L.W., Zachmann, D.W., 2004. Handbook for Predicting Stream Meander Migration. Transportation Research Board, N.C.H.R. Program, p. 107.

Latrubesse, E.M., 2008. Patterns of anabranching channels: the ultimate end-member adjustment of mega rivers. Geomorphology 101, 130–145.

Lauer, J.W., Parker, G., 2008a. Modeling framework for sediment deposition, storage, and evacuation in the floodplain of a meandering river: theory. Water Resour. Res. 44.

Lauer, J.W., Parker, G., 2008b. Net local removal of floodplain sediment by river meander migration. Geomorphology 96, 123–149.

Lawler, D., 1986. River bank erosion and the influence of frost: a statistical examination. Trans. Inst. Br. Geogr. 227–242.

Lawler, D.M., 1993. The measurement of river bank erosion and lateral channel change: a review. Earth Surf. Process. Landf. 18, 777–821.

Legleiter, C.J., Kyriakidis, P.C., 2006. Forward and inverse transformations between Cartesian and channel-fitted coordinate systems for meandering rivers. Math. Geol. 38, 927–958.

Leopold, L.B., 1973. River channel change with time: an example address as retiring president of the Geological Society of America, Minneapolis, Minnesota, November 1972. Geol. Soc. Am. Bull. 84, 1845–1860.

Leys, K.F., Werritty, A., 1999. River channel planform change: software for historical analysis. Geomorphology 29, 107–120.

Marra, W.A., Kleinhans, M.G., Addink, E.A., 2014. Network concepts to describe channel importance and change in multichannel systems: test results for the Jamuna River, Bangladesh. Earth Surf. Process. Landf. 39, 766–778.

McFeeters, S., 1996. The use of the Normalized Difference Water Index (NDWI) in the delineation of open water features. Int. J. Remote Sens. 17, 1425–1432.

Mertes, L.A.K., Dunne, T., Martinelli, L.A., 1996. Channel–floodplain geomorphology along the Solimoes–Amazon River, Brazil. Geol. Soc. Am. Bull. 108, 1089–1107.

Merwade, V.M., 2007. An automated GIS procedure for delineating river and lake boundaries. Trans. GIS 11, 213–231.

Micheli, E.R., Kirchner, J.W., 2002. Effects of wet meadow riparian vegetation on streambank erosion. 1. Remote sensing measurements of streambank migration and erodibility. Earth Surf. Process. Landf. 27, 627–639.

Micheli, E., Larsen, E., 2011. River channel cutoff dynamics, Sacramento River, California, USA. River Res. Appl. 27, 328–344.
Micheli, E., Kirchner, J., Larsen, E., 2004. Quantifying the effect of riparian forest versus agricultural vegetation on river meander migration rates, Central Sacramento River, California, USA. River Res. Appl. 20, 537–548.
Mount, N., Louis, J., 2005. Estimation and propagation of error in measurements of river channel movement from aerial imagery. Earth Surf. Process. Landf. 30, 635–643.
Mount, N., Louis, J., Teeuw, R., Zukowskyj, P., Stott, T., 2003. Estimation of error in bankfull width comparisons from temporally sequenced raw and corrected aerial photographs. Geomorphology 56, 65–77.
Mount, N.J., Tate, N.J., Sarker, M.H., Thorne, C.R., 2012. Evolutionary, Multi-Scale Analysis of River Bank Line Retreat Using Continuous Wavelet Transforms: Jamuna River. Bangladesh, Geomorphology.
Nanson, R.A., 2010. Flow fields in tightly curving meander bends of low width-depth ratio. Earth Surf. Process. Landf. 35, 119–135.
Nanson, G.C., Hickin, E.J., 1983. Channel migration and incision on the Beatton River. J. Hydraul. Eng. 109, 327–337.
Nanson, G.C., Hickin, E.J., 1986. A statistical analysis of bank erosion and channel migration in western Canada. Geol. Soc. Am. Bull. 97, 497–504.
Nanson, G.C., Page, K., 1983. Lateral accretion of fine-grained concave benches on meandering rivers. Modern and Ancient Fluvial Systems (Special Publication 6 of the IAS), p. 133.
Nash, J., Sutcliffe, J., 1970. River flow forecasting through conceptual models part I—a discussion of principles. J. Hydrol. 10, 282–290.
Notebaert, B., Piégay, H., 2013. Multi-scale factors controlling the pattern of floodplain width at a network scale: the case of the Rhône basin, France. Geomorphology 200, 155–171.
Parker, G., Shimizu, Y., Wilkerson, G., Eke, E., Abad, J., Lauer, J., Paola, C., Dietrich, W., Voller, V., 2011. A new framework for modeling the migration of meandering rivers. Earth Surf. Process. Landf. 36, 70–86.
Pavelsky, T.M., Smith, L.C., 2008. RivWidth: a software tool for the calculation of river widths from remotely sensed imagery. IEEE Geosci. Remote Sens. Lett. 5, 70–73.
Paz, A.R., Collischonn, W., 2007. River reach length and slope estimates for large-scale hydrological models based on a relatively high-resolution digital elevation model. J. Hydrol. 343, 127–139.
Peixoto, J.M.A., Nelson, B.W., Wittmann, F., 2009. Spatial and temporal dynamics of river channel migration and vegetation in central Amazonian white-water floodplains by remote-sensing techniques. Remote Sens. Environ. 113, 2258–2266.
Perkins, S.J., Edlund, K., Esch-Mosher, D., Eads, D., Harvey, N., Brumby, S., 2005. Genie Pro: robust image classification using shape, texture, and spectral information. Proceedings of SPIE *5806*, 139–148.
Pizzuto, J., 2009. An empirical model of event scale cohesive bank profile evolution. Earth Surf. Process. Landf. 34, 1234–1244.
Priestnall, G., Aplin, P., 2006. Spatial and temporal remote sensing requirements for river monitoring. Int. J. Remote Sens. 27, 2111–2120.
Quackenbush, L.J., 2004. A review of techniques for extracting linear features from imagery. Photogramm. Eng. Remote Sens. 70, 1383–1392.
Richard, G.A., Julien, P.Y., Baird, D.C., 2005. Statistical analysis of lateral migration of the Rio Grande, New Mexico. Geomorphology 71, 139–155.
Rozo, M.G., Nogueira, A.C., Castro, C.S., 2014. Remote sensing-based analysis of the planform changes in the Upper Amazon River over the period 1986–2006. J. S. Am. Earth Sci. 51, 28–44.
Serra, P., Pons, X., Sauri, D., 2003. Post-classification change detection with data from different sensors: some accuracy considerations. Int. J. Remote Sens. 24, 3311–3340.
Shields, F.D., Simon, A., Steffen, L.J., 2000. Reservoir effects on downstream river channel migration. Environ. Conserv. 27, 54–66.
Smith, L.C., Pavelsky, T.M., 2008. Estimation of river discharge, propagation speed, and hydraulic geometry from space: Lena River, Siberia. Water Resources Research 44.
Snow, R.S., 1989. Fractal sinuosity of stream channels. pure and applied geophysics *131*, 99–109.
Thorne, C.R., Tovey, N.K., 1981. Stability of composite river banks. Earth Surf. Process. Landf. 6, 469–484.
Van Niel, T.G., McVicar, T.R., Li, L., Gallant, J.C., Yang, Q., 2008. The impact of misregistration on SRTM and DEM image differences. Remote Sens. Environ. 112, 2430–2442.
Verbyla, D., Boles, S., 2000. Bias in land cover change estimates due to misregistration. Int. J. Remote Sens. 21, 3553–3560.
Vietz, G.J., Rutherfurd, I.D., Stewardson, M.J., Finlayson, B.L., 2012. Hydrodynamics and sedimentology of concave benches in a lowland river. Geomorphology 147, 86–101.
Wang, H., Ellis, E.C., 2005. Image misregistration error in change measurements. Photogramm. Eng. Remote Sens. 71, 1037–1044.
Wheaton, J.M., Brasington, J., Darby, S.E., Sear, D.A., 2010. Accounting for uncertainty in DEMs from repeat topographic surveys: improved sediment budgets. Earth Surf. Process. Landf. 35, 136–156.
Winterbottom, S.J., Gilvear, D.J., 2000. A GIS-based approach to mapping probabilities of river bank erosion: regulated River Tummel, Scotland. Regulated Rivers: Research & Management 16, 127–140.
Wolman, M., 1959. Factors influencing erosion of a cohesive river bank. Am. J. Sci. 257, 204–216.
Wolman, M.G., Leopold, L.B., 1957. River Flood Plains; Some Observations on Their Formation.
Woodyer, K., 1975. Concave-bank benches on Barwon River, NSW. Aust. Geogr. 13, 36–40.
Wynn, T., Henderson, M., Vaughan, D., 2008. Changes in streambank erodibility and critical shear stress due to subaerial processes along a headwater stream, southwestern Virginia, USA. Geomorphology 97, 260–273.
Xu, H., 2006. Modification of normalised difference water index (NDWI) to enhance open water features in remotely sensed imagery. Int. J. Remote Sens. 27, 3025–3033.
Yamazaki, D., O'Loughlin, F., Trigg, M.A., Miller, Z.F., Pavelsky, T.M., Bates, P.D., 2014. Development of the global width database for large rivers. Water Resour. Res. 50, 3467–3480.
Yumoto, M., Ogata, T., Matsuoka, N., Matsumoto, E., 2006. Riverbank freeze–thaw erosion along a small mountain stream, Nikko volcanic area, central Japan. Permafr. Periglac. Process. 17, 325–339.
Zar, J.H., 1999. Biostatistical Analysis. fourth ed. Prentice-Hall, Inc., New Jersey.
Zolezzi, G., Luchi, R., Tubino, M., 2012a. Modeling morphodynamic processes in meandering rivers with spatial width variations. Rev. Geophys. 50, RG4005.
Zolezzi, G., Luchi, R., Tubino, M., 2012b. Modeling morphodynamic processes in meandering rivers with spatial width variations. Rev. Geophys. 50.